



DEPARTMENT OF CHEMICAL ENGINEERING

TKP4580 - CHEMICAL ENGINEERING, SPECIALIZATION PROJECT

---

# Model development and optimization for flexible operation of renewable Hydrogen production

---

Supervisor: Johannes Jäschke  
Cosupervisor: Lucas Cammann  
Author: Hanne Marie Grov

December 16, 2022

# Abstract

As of today, the conventional production of hydrogen is based on fossil fuels, using a steam-methane reformer with natural gas. However, utilizing such fossil fuels contributes to the ongoing climate changes. Alternatively, green hydrogen production powered by wind turbines will contribute to environmental innovation for several chemical processes. However, compared to traditional fuels such as natural gas, wind power will vary significantly depending on wind velocities. This project aims to examine optimal operating conditions for a large-scale green hydrogen plant based on a steady-state model. The model mainly consists of three electrolyzers powered by wind turbines. The electrolyzers split water molecules into hydrogen and oxygen. Due to the explosive nature of this mixture, also called the hydrogen-to-oxygen ratio (HTO), the concentration should be operated within a maximal limit. If the HTO exceeds this limit, the plant shuts down. Hence, operating with low measurements of HTO is required.

To achieve this, it is formalized a nonlinear optimization problem (NLP) to maximize the production of Hydrogen with model constraints. The NLP is further solved with minimal, maximal, and flexible setpoints for the constraints using realistic wind data. This data is simulated through `renewables.ninja` with capacities at 5 MW, 6 MW and 7 MW[1]. As a result, the total production through 2019 is documented, for each of the capacities and different setpoints for the constraints. Compared to minimal setpoints with a capacity at 5 MW, the total production is increased with 2.8% for maximal setpoints and 60.2% for flexible setpoints. However, optimizing with maximal setpoints leads to downtime for all capacities due to the HTO limit being exceeded.

The model is also optimized for different capacities, where the constraints are set to their flexible setpoints. Hence, compared to the lower capacity at 5 MW, the total production increased by 15.3% with 6 MW and 27.8% with 7 MW. Meanwhile, capacity at 5 MW was found to be most profitable with a cost of capital larger than 7.241%. For further work, the degradation of the electrolyzers should be investigated due to unexpected changes in the cooling water. Additionally, a dynamic model should be developed with implemented control structures.

# Contents

<b>1</b>	<b>Introduction</b>	<b>10</b>
<b>2</b>	<b>Theoretical Background</b>	<b>11</b>
2.1	Model description . . . . .	11
2.1.1	Alkaline water electrolysis . . . . .	11
2.2	Model equations . . . . .	15
2.2.1	Electrolyzer . . . . .	15
2.2.2	Separators . . . . .	18
2.2.3	Buffer tank . . . . .	19
2.2.4	Heat exchangers . . . . .	20
2.2.5	Compressor duty . . . . .	21
2.3	Wind turbine power . . . . .	21
2.3.1	Weibull distribution . . . . .	21
2.3.2	The present value method . . . . .	22
<b>3</b>	<b>Method and Model Implementation</b>	<b>23</b>
3.1	Optimization setup . . . . .	23
3.2	Wind turbine data . . . . .	24
3.2.1	Profitability estimation . . . . .	25
<b>4</b>	<b>Results and Discussion</b>	<b>26</b>
4.1	Active constraint regions . . . . .	26
4.2	Performance parameters . . . . .	28
4.2.1	Bubble formation . . . . .	29
4.3	Weibull distribution . . . . .	30
4.4	Flexible and fixed constraints . . . . .	31
4.5	Profitability estimation . . . . .	34
<b>5</b>	<b>Conclusion and Further Research</b>	<b>36</b>

<b>A Appendix</b>	<b>42</b>
A.1 Performance Parameters . . . . .	42
A.2 Julia Code . . . . .	42
A.2.1 Main . . . . .	42
A.2.2 Model . . . . .	45
A.3 Simulation . . . . .	49
A.3.1 Parameters . . . . .	51
A.3.2 Performance parameters . . . . .	52
A.3.3 The net present value . . . . .	53
A.3.4 Wind data . . . . .	53
A.3.5 Absolute and Weighted production rate . . . . .	55

# List of Figures

2.1	Plant design with three electrolyzers denoted as stack 1, 2, and 3. The liquid-gas separators, buffer tank, two compressors, and storage tanks are also included. The power, $P_{net}$ , is supplied through wind turbines and represented by the dashed lines, while the filled lines are mass flows $\dot{m}$ [ $\text{kg s}^{-1}$ ] and molar flows $\dot{n}$ [ $\text{mol/s}$ ]. The plant is based on Lucas Cammann[2] and designed in Inkscape[3]. . . . .	12
2.2	The cell structure in one of the electrolyzer stacks with cathode and anode surfaces. The black arrows presents molar flows, $\text{mol s}^{-1}$ , while the red arrows and components present the course of the cell reaction. The green arrows point to the bubbles, cell membrane, and electrolyte surface which consists of nickel. The cell drawing is inspired by Lucas Cammann[2] and designed in Inkscape[3]. . . . .	17
2.3	Inputs and outputs for one electrolyzer. The power input is $P_{net}$ illustrated with a dashed line, while mass flows are represented with black lines and the heat transfer with red lines. The electrolyzer drawing is inspired by Lucas Cammann[2] and designed in Inkscape[3]. . . . .	18
2.4	Liquid-gas separator at the anodic electrode. $\dot{n}_i$ is the molar flow of component $i$ . $g$ and $l$ denote gas and liquid phase respectively. The drawing is inspired by Lucas Cammann[2] and designed in Inkscape[3]. . . . .	19
2.5	Heat exchanger temperature profile and energy and mass flows. The drawing is inspired by Lucas Cammann[2] and designed in Inkscape[3]. . . . .	21
3.1	The map of Porsgrunn and Hovde is found from renewables.ninja[1] and edited in Inkscape[3]. . . . .	25
4.1	Active constraint regions for electrolyzer 1 without bubble formation. The power input, $P_{net}$ ranges from 0.03 MW to 6.5 MW. The circles mark the solution to the NLP in equation (3.3). $g/g_{max}$ is the ratio of the solution for the current power input, $g$ , and the maximal setpoint, $g_{max}$ [2]. . . . .	27

4.2	Active constraint regions for electrolyzer 1 with bubble formation. The power input, $P_{net}$ ranges from 0.03 MW to 6.5 MW. The circles mark the solution to the NLP in equation (3.3). $g/g_{max}$ is the ratio of the solution for the current power input, $g$ , and the maximal setpoint, $g_{max}[2]$ . . . . .	28
4.3	Active constraint regions for electrolyzer 2 and 3 without bubble formation. The power input, $P_{net}$ ranges from 0.03 MW to 6.5 MW. The circles mark the solution to the NLP in equation (3.3). $g/g_{max}$ is the ratio of the solution for the current power input, $g$ , and the maximal setpoint, $g_{max}[2]$ . . . . .	29
4.4	Active constraint regions for electrolyzer 2 and 3 with bubble formation. The power input, $P_{net}$ ranges from 0.03 MW to 6.5 MW. The circles mark the solution to the NLP in equation (3.3). $g/g_{max}$ is the ratio of the solution for the current power input, $g$ , and the maximal setpoint, $g_{max}[2]$ . . . . .	29
4.5	Bubble formation for each electrolyzer, $\theta[j]$ , with power input, $P_{net}$ , ranging from 0.03 MW to 6.5 MW. . . . .	30
4.6	Weekly mean of the generated wind power at Hovde in 2019. The capacity for the simulation is set to 6 MW, and simulated using <i>renewables.ninja</i> [1]. . . . .	31
4.7	The weibull distribution for the simulated wind power at Hovde in 2019 with capacity at 6 MW. The weibull function, $f$ , is presented in (2.33). . . . .	31
4.8	The weibull distribution for the simulated wind power at Hovde in 2019 with capacity at 5 MW. . . . .	31
4.9	The weibull distribution for the simulated wind power at Hovde in 2019 with capacity at 7 MW. . . . .	31
4.10	Absolute and weighted production rate for minimal, maximal, and flexible setpoints with a capacity of 6 MW. . . . .	32
4.11	Absolute and weighted production rate for minimal, maximal, and flexible setpoints with a capacity of 5 MW. . . . .	33
4.12	Absolute and weighted production rate for minimal, maximal, and flexible setpoints with a capacity of 7 MW. . . . .	33
4.13	Downtime for production operating at maximal setpoints through 2019. 5, 6, and 7 MW yields 7417, 6594 and 5581 hours respectively. . . . .	34
4.14	The present value profile for operation and investment at 5 MW, 6 MW, and 7 MW. The lifetime of the projects is set to 15 years. . . . .	35

# List of Tables

4.1	The integrated absolute and weighted production rate of hydrogen for operating at maximal, minimal, and flexible setpoints with capacities at 5 MW, 6 MW, and 7 MW. The total production of hydrogen through 2019 is also included. . . . .	34
A.1	The performance parameters implemented for each of the electrolyzers according to Rizwan[4]. . . . .	42





## List of Symbols

Symbol	Definition	Units
$P_{net}$	Power inputs from wind turbines	MW
$\dot{m}$	Mass flow	$kg/s$
$\dot{n}$	Molar mass flow	$mol/s$
$\Delta G$	Gibbes free energy	$kJ/mol$
$z$	The number of electrones	
$F$	Faraday's constant	$C/mol$
$U_{rev}$	Reversible cell voltage	V
$U_{tn}$	Thermoneutral cell voltage	V
$T^{El}$	Temperature in electrolyte	K
$A$	Area of electrolyzer	$m^2$
$I$	Current	$A/m^2$
$r_1$	The ohmic resistance parameter	$\Omega m^2$
$r_2$	The ohmic resistance parameter	$\Omega m^2/^\circ C$
$t_1$	Overvoltage coefficient	$m^2/A$
$t_2$	Overvoltage coefficient	$m^2^\circ C/A$
$t_3$	Overvoltage coefficient	$m^2^\circ C^2/$
$I_{eff}$	Effective current density	$A/m^2$
$\theta$	Bubble coverage	
$v$	Flow velocity of the electrolyte	$m/s$
$K$	Fitting parameter	
$\rho$	Density	$kg/m^3$
$A$	Areal	$m^2$
$M$	Molar mass	$g/mol$
$D$	Diffusivity	$m^2/s$
$S$	Solubility	$mol/L$
$nc$	The number of cells	
$L_m$	The thickness of the membrane	$m$
$\eta_F$	Faraday's efficiency	

---

Symbol	Definition	Units
$f_1$	Performance parameter	$mA^2/cm^4$
$f_2$	Performance parameter	
$\dot{Q}$	Heat transfer	W
$C_t$	Overall thermal capacity	$J/K$
$C_p$	Heat capacity	$J/K$
$A_s$	Active electrolyte area	$m^2$
$h_c$	Convective heat transfer	$W/K$
$\sigma$	Stefan-Boltzmann's constant	$W/m^2K^4$
$H$	Henry's solubility	$atm^{-1}$
$P_{sys}$	The pressure of the system	$bar$
$\eta_{comp}$	Compressor efficiency	
$\lambda$	Scale parameter	
$k$	Shape parameter	
$r$	Cost of capital	
$y$	Years	
$C_0$	Investment cost	
$CF$	Cash flows	

---

## Introduction

Hydrogen is currently in high demand, as it is being utilized as a fuel, energy storage, and raw material in a wide range of chemical processes. As an example, the Haber-Bosh process utilizes hydrogen in the production of fertilizer which is essential for today's global food demand[5]. Currently, the conventional production of hydrogen is based on fossil fuels, using a steam-methane reformer with natural gas. Utilizing such fossil fuels is not only environmentally harmful as it contributes to the ongoing climate changes, but it also poses economical risks due to today's varying fuel prices. According to an article by SINTEF, the current price of natural gas in 2022 has increased by ten times since 2019[6]. In light of these challenges, efficient and green hydrogen production has gained significant interest in research communities and the chemical industry worldwide.

Going forward, green hydrogen production is likely to grow as technology allows for more robust and efficient production. Compared to conventional production, green hydrogen only utilizes renewable energy sources such as wind, solar, and water power. Thus, the production is also independent of the fluctuating fuel prices, which makes it highly attractive. However, in spite of the definite advantages of green hydrogen, the technology is also fairly new and brings forth trade-offs.

This project aims to model a realistic plant for green hydrogen production for the purpose of finding optimal operating conditions by investigating these trade-offs. The model consists of three electrolyzers with a total nominal power consumption of 6 MW. In the electrolyzers, water molecules are split into hydrogen and oxygen. The hydrogen-to-oxygen ratio, often referred to as the HTO, poses substantial risks as this mixture is known to be explosive at greater ratios. Thus, in order to operate safely, it is crucial to keep the HTO below a maximal limit. Additionally, the bubble formation of gas on the electrolyte surface and the pressure of the system affect the efficiency of production. A nonlinear optimization problem is therefore solved with model constraints for critical parameters such as the HTO, flowrate, and pressure. Further, different setpoints for the constraints are utilized for the optimization problem, which is further solved using realistic wind data. This data is simulated for different capacities of wind power, where production rate and total production are documented. Finally, an estimate of the profitability of production and installation with different capacities is found.

## Theoretical Background

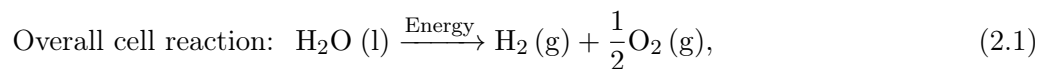
To analyze the behavior of a renewable hydrogen plant, a steady-state model is established based on theoretical model equations. The model in this project is based on the model equations by Lucas Cammann[2].

### 2.1 Model description

The hydrogen plant is presented as a system with three electrolyzers, represented by the three stacks in Figure 2.1[2]. Each stack contains 230 cells with a nominal power load of 2 MW in total for each stack[7]. The power,  $P_{net}$ , is assumed to be based on a wind turbine park connected to the Hydrogen plant. The product gas of each electrolyzer is stored after separating the gas from the liquid phase through the six liquid-gas separators. The liquid phase is further recycled through the buffer tank. In the buffer tank, the liquid phase is mixed with the water make-up stream,  $\dot{m}_{makeup,H_2O}^{el}$ , which reestablishes the lye concentration. Further, this lye is compressed and cooled before reentering the electrolyzers. A more detailed description of each unit is presented in section 2.2.

#### 2.1.1 Alkaline water electrolysis

The alkaline water electrolysis process occur in an electrolyzer, where electric current is utilized to split water molecules to hydrogen and oxygen. Figure 2.2 presents the cell structure inside the electrolyzers. The overall reaction in the electrolyzer is presented as:



where the applied energy is the cell voltage, or reversible voltage. The process also requires an electrolyte solution which transports the electrons. For water electrolysis a lye solution with 30 wt% potassium hydroxide (KOH) is commonly utilized due to it's efficient conductivity at temperatures between 50 °C and 80 °C[8].

As illustrated in Figure 2.2, the electrolyzer further constitutes of two electrodes separated by the cell membrane. Nickel is often used as the material of the electrodes, due to it's favorable properties

such as high conductivity and resistance of corrosion. The electrodes are additionally categorized as anode and cathode. At the cathode, water is reduced to hydrogen and hydroxide ions, while further oxidation of the hydroxide ions to oxygen and water takes place at the anode:

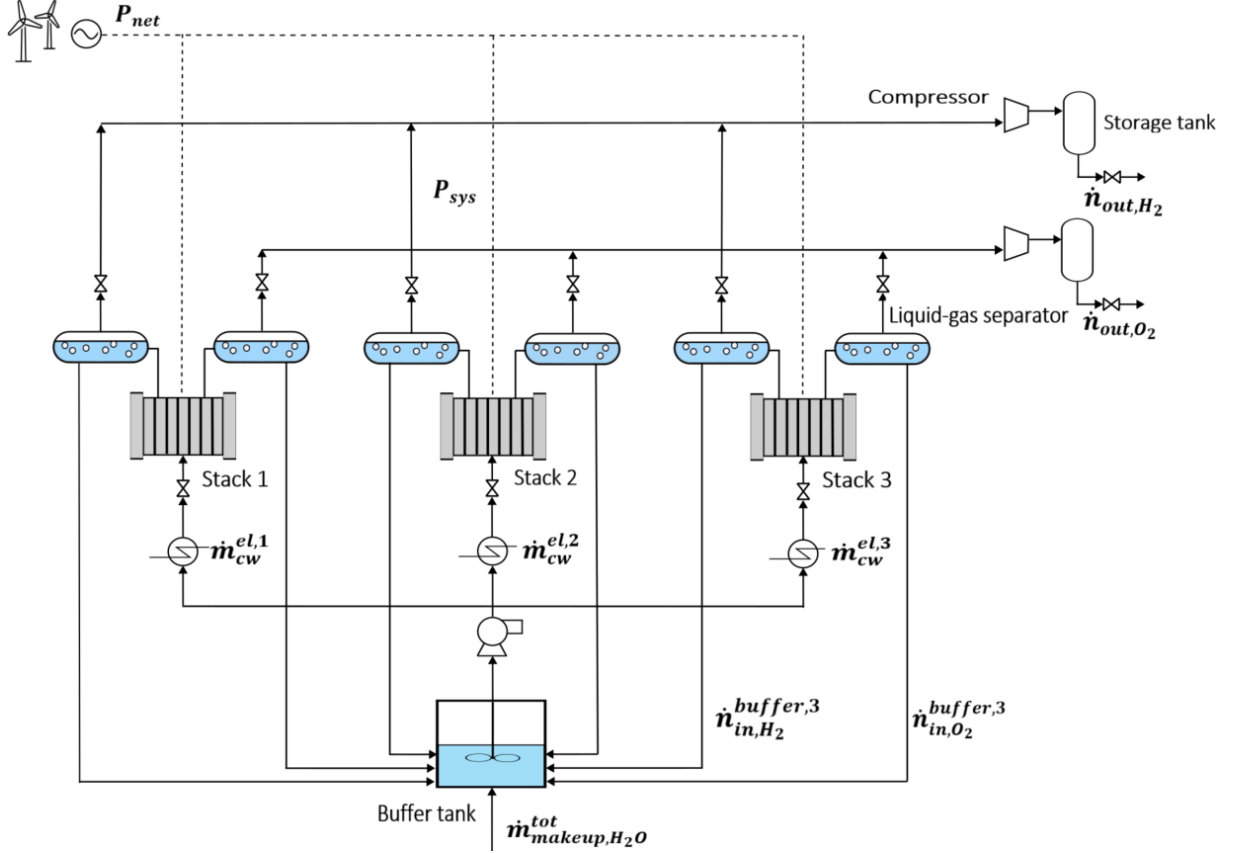
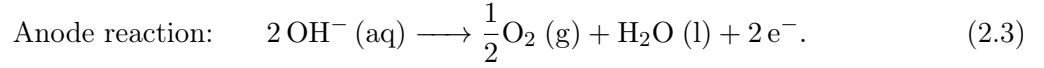
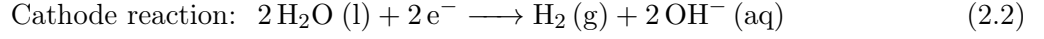


**Figure 2.1:** Plant design with three electrolyzers denoted as stack 1, 2, and 3. The liquid-gas separators, buffer tank, two compressors, and storage tanks are also included. The power,  $P_{net}$ , is supplied through wind turbines and represented by the dashed lines, while the filled lines are mass flows  $\dot{m}$  [ $\text{kg s}^{-1}$ ] and molar flows  $\dot{n}$  [ $\text{mol/s}$ ]. The plant is based on Lucas Cammann[2] and designed in Inkscape[3].

### Cell voltage

The cell voltage can be described through the thermodynamic model by Øystein Ulleberg, and is based on the following assumptions[9];

- Hydrogen and oxygen is modeled as ideal gases.
- Water is defined as an incompressible fluid.

- The gas and liquid phases are separate.

These assumptions yields the applied cell voltage expressed through the Gibbs free energy,  $\Delta G_{\text{reac}}$ , for the overall reaction in equation (2.1). Gibbs free energy is the change in enthalpy,  $\Delta H_{\text{reac}}$ , entropy,  $\Delta S_{\text{reac}}$ , and thermodynamic temperature  $T$ :

$$\Delta G_{\text{reac}} = \Delta H_{\text{reac}} - T \cdot \Delta S_{\text{reac}}. \quad (2.4)$$

For standard temperature and pressure, the overall water splitting reaction is non-spontaneous as the Gibbs free energy in equation (2.4) is positive,  $\Delta G^\circ = 237 \text{ kJ mol}^{-1}$ . Thus, the electrolysis requires some electrical energy, or emf, to split the water molecules. This energy is further described by the reversible cell voltage,  $U_{\text{rev}}$ :

$$U_{\text{rev}} = -\frac{\Delta G_{\text{reac}}}{z \cdot F}, \quad (2.5)$$

where  $z$  is the number of electrons and  $F$  is Faraday's constant set to  $96.485 \text{ C mol}^{-1}$ . Additionally, the thermoneutral cell voltage,  $U_{\text{tn}}$ , represents the total energy demand for the cell reaction,  $\Delta G_{\text{reac}}$ , and the energy needed to maintain the thermodynamic temperature,  $T\Delta S_{\text{reac}}$ . Thus, the electrolysis must operate with a cell voltage above thermoneutral cell voltage[10]. The expression for the thermoneutral voltage can be found through the reaction enthalpy,  $\Delta H_{\text{reac}} = \Delta G_{\text{reac}} + T\Delta S_{\text{reac}}$ , assuming no heat is lost to the surroundings[9]:

$$\implies U_{\text{tn}} = -\frac{\Delta H_{\text{reac}}}{z \cdot F}. \quad (2.6)$$

According to Øystein Ulleberg [9], the thermoneutral cell voltage is close to 1.48 V through the entire temperature span of the electrolyzers (20 °C to 80 °C).

The reversible cell voltage is the minimum voltage required for the electrolysis to take place. In a realistic process there exists irreversibilities which causes energy losses and limits the cell efficiency. These irreversibilities constitutes of parasitic current and overvoltages[11]. Hence, the actual supplied cell voltage is defined as:

$$U = U_{\text{rev}} + \underbrace{U_{\text{ohm}} + U_{\text{act}} + U_{\text{con}}}_{\text{overvoltage}}. \quad (2.7)$$

As the expression suggest, physical irreversibilities causes ohmic, activation and concentration overvoltage, denoted as *ohm*, *act* and *con* respectively. Ohmic overvoltage,  $U_{\text{ohm}}$ , is the voltage loss due to resistance in electron transport[11]. Considering Ohm's law,  $U = I \cdot R$ , the resistance changes linearly with increasing currents. In contrast to this linear behavior, the activation overvoltage,  $U_{\text{act}}$ , behaves nonlinear and logarithmic, and is described as the required electrode energy for charge transfer between the electrodes. Finally, the concentration overvoltage,  $U_{\text{con}}$ , is the resistance due to mass transfer. However, this overvoltage is typically neglected as it is insignificant compared to the two other overvoltages[11].

The model developed in this project utilizes the empirical current-voltage (I-U) expression to describe the cell voltage in the electrolyzers[9]:

$$U = U_{rev} + \frac{r_1 + r_2 T^{EL}}{A} I + s \log \left( \left( t_1 + \frac{t_2}{T^{EL}} + \frac{t_3}{T^{EL^2}} \right) \frac{I}{A} + 1 \right), \quad (2.8)$$

where  $A$  is the area of the electrode,  $T^{EL}$  is the electrolyzer temperature and  $I$  is the current in A/m<sup>2</sup>. Moreover,  $r$  is defined as the ohmic resistance parameter, while  $t$  and  $s$  represents the overvoltage coefficients. These values are found through literature and influence the efficiency of the electrolyzer as they often increase with ageing of the electrolyzer[11]. The set values utilized for this project is presented in Table A.1, see Appendix A.1.

## HTO

The products of the alkaline water electrolysis is hydrogen and oxygen gas as presented in equation (2.1). These gases are known to be explosive at mixtures with 4 to 96 vol.% of gas contamination [8]. Thus, the gas purity of the alkaline water electrolysis must be carefully controlled. A threshold value of 2 vol.% is therefore included in the model which ensures shutdown of the plant. The gas contamination can be defined as[2],

$$HTO = \frac{\dot{n}_{out,H_2}^{sep,an}}{\dot{n}_{out,O_2}^{sep,an}}, \quad (2.9)$$

which is the hydrogen-to-oxygen ratio (HTO) measured at the anodic separator. Hence, higher levels of HTO represents higher gas contamination in the system which may lead to unsafe operations that further results in shutdown of the plant.

According to Jörn Brauns[8], the HTO level increases with decreasing current densities. This is caused by the electrolyte mixing remaining constant, while the production rate is decreased due to the decrease in current densities. Likewise, increased pressure will increase the HTO level. This is due to the solubility of both  $O_2$  and  $H_2$  rising with higher pressures[12], which further causes cross-contamination through the cell membrane, see Figure 2.2[13]. Lastly, the electrolyte mixing also increases the HTO level. Thus, to keep the HTO level within the threshold value at 2 vol.% and prevent shutdown, the current densities, the pressure of the system and the electrolyte mixing demands careful operation.

## Bubble formation

During the electrolysis of water, bubbles of both hydrogen and oxygen gas are formed on the surfaces of the electrodes, see Figure 2.2. These gas bubbles arise from the cell reactions at the cathode and anode. As the reaction progresses, the bubbles grow due to the gas accumulation and then detach from the electrode surfaces. These bubble formations are undesirable as electrical resistance is increased and results in ohmic loss. This is due to the bubbles blocking off contact between the electrolyte and the electrode surface, hence hindering ionic transfer[14]. Thus, the fraction of

bubbles on the surface,  $\theta$ , causes an inactive electrolyte surface, decreasing the effective current density,  $I_{eff}$ , as presented in the following equation:

$$I_{eff} = I \cdot (1 - \theta), \quad (2.10)$$

where  $I$  represents the overall current density [15]. Accordingly, the bubble formation depends on the rate of gas evolution, which also depends on the current density, as stated by Vogt [16]. The bubble formation is therefore directly influenced by the current density. Hence, the stagnant bubble coverage, assuming no flow velocity of the electrolyte  $v = 0 \text{ m s}^{-1}$ , is found through [16]:

$$\theta_0 = \left[ \frac{I}{I_{\theta \rightarrow 1}} \right]^m, \quad (2.11)$$

where  $I_{\theta \rightarrow 1}$  denotes the maximum current density which is found through experimental data, and  $m$  is set to 0.3. However, the active bubble formation on the electrolyte surface depends on the electrolyte velocity  $v$  through the electrode [17]:

$$\theta = \frac{\theta_0}{[1 + (K \cdot v)^2]^2}, \quad (2.12)$$

where  $K$  denotes an additional fitting parameter set to 8. The electrolyte velocity is further defined as:

$$v = \frac{\dot{m}_{lye,in}^{el}}{\rho_{lye} \cdot A_{lyeflow}}, \quad (2.13)$$

where  $\rho_{lye}$  is the density of the lye, found to be  $1258.2 \text{ kg/m}^3$ , and the area of the electrode surface,  $A_{lyeflow}$ , is set to be  $3.63 \text{ m}^2$  [7].

## 2.2 Model equations

In order to simulate the green hydrogen plant presented in Figure 2.1, the steady-state equations are implemented in the model using the equations presented below. Both the mass and energy balances for each unit are included, which are based on the work by Lucas Cammann [2].

### 2.2.1 Electrolyzer

The model equations are similar for each of the three electrolyzers, see Figure 2.3. Thus, mass and molar flows for electrolyzer 1, 2 and 3 are denoted by  $j$ . The overall mass balance of electrolyzer  $j$  is defined as:

$$\begin{aligned} \frac{dm^{el,j}}{dt} &= \sum \dot{m}_{in}^j - \sum \dot{m}_{out}^j \\ &= M_{H_2} (2\dot{n}_{in,H_2}^j - \dot{n}_{out,H_2}^{cat,j} - \dot{n}_{out,H_2}^{an,j}) + M_{O_2} (2\dot{n}_{in,O_2}^j - \dot{n}_{out,O_2}^{cat,j} - \dot{n}_{out,O_2}^{an,j}) \\ &\quad + \dot{m}_{lye,in}^{el,j} - \dot{m}_{lye,out}^{el,j}, \end{aligned} \quad (2.14)$$



where  $M_i$  is the molar mass of component  $i$ . Further, the molar component balances, see Figure 2.2, can be described as the following:

$$\begin{aligned}
\frac{dn_{H_2}^{cat,j}}{dt} &= \dot{n}_{in,H_2}^j + \dot{n}_{r,H_2}^j - \dot{n}_{diff,H_2}^j - \dot{n}_{out,H_2}^{cat,j} \\
\frac{dn_{O_2}^{cat,j}}{dt} &= \dot{n}_{in,O_2}^j + \dot{n}_{diff,O_2}^j - \dot{n}_{out,O_2}^{cat,j} \\
\frac{dn_{H_2}^{an,j}}{dt} &= \dot{n}_{in,H_2}^j + \dot{n}_{diff,H_2}^j - \dot{n}_{out,H_2}^{an,j} \\
\frac{dn_{O_2}^{an,j}}{dt} &= \dot{n}_{in,O_2}^j + \dot{n}_{r,O_2}^j - \dot{n}_{diff,O_2}^j - \dot{n}_{out,O_2}^{an,j},
\end{aligned} \tag{2.15}$$

where the anodic and cathodic balances are denoted with subscript *an* and *cat* respectively. Likewise, the subscripts *in* and *out* denotes the inflow, or the recycled lye, into the electrolyzer and the outflow, or the product flows respectively. Finally, *r* and *diff* denotes the reactive and diffusive fluxes respectively, calculated with the following equations:

$$\dot{n}_{r,i}^j = \eta_F^j \frac{n_c I_{eff}^j A^{el,j}}{zF} \tag{2.16}$$

$$\dot{n}_{diff,i}^j = \frac{P_{sys} S_i D_i A^{el,j}}{L_m}. \tag{2.17}$$

$A^{el,j}$  represents the active surface area on the electrolyte  $j$ ,  $n_c$  is the number of cells while  $P_{sys}$  is the system pressure. Additionally,  $S_i$  is the solubility found through Henry's law and  $D_i$  is the diffusivity of component  $i$ . The number of transferred electrons is denoted as  $z$ , while  $L_m$  is set as the thickness of the membrane. Finally,  $\eta_F^j$  is the expression for Faraday's efficiency, which describes the ratio between the actual and maximum theoretical production of hydrogen. Empirically, the expression can be formulated as[9]:

$$\eta_F^j = \frac{\left(I_{eff}^j\right)^2}{f_1^j + \left(I_{eff}^j\right)^2} f_2^j, \tag{2.18}$$

where  $f_1^j$  and  $f_2^j$  is parameters related to the efficiency of the electrolyzer, see Appendix A.1 for further description.

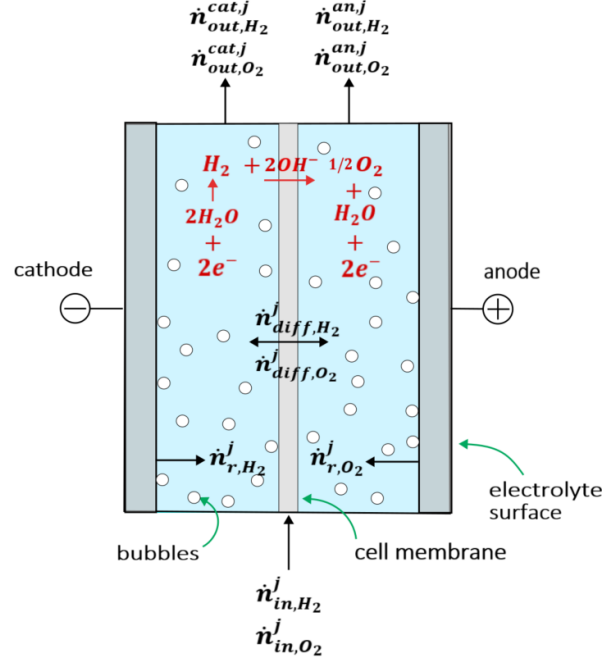


**Figure 2.2:** The cell structure in one of the electrolyzer stacks with cathode and anode surfaces. The black arrows presents molar flows,  $\text{mol s}^{-1}$ , while the red arrows and components present the course of the cell reaction. The green arrows point to the bubbles, cell membrane, and electrolyte surface which consists of nickel. The cell drawing is inspired by Lucas Cammann[2] and designed in Inkscape[3].

As stated by Georgios Sakas[18], the energy balance of the electrolyzers can be simplified as:

$$\frac{dU^{el}}{dt} = \sum \dot{Q}_{in} - \sum \dot{Q}_{out} = \dot{Q}_{loss} - \dot{Q}_{conv} - \dot{Q}_{cond}. \quad (2.19)$$

The generated heat,  $\dot{Q}_{loss}$ , is caused by the difference in the cell voltage,  $U_k$ , and the thermoneutral cell voltage,  $U_{tn}$ , see equation (2.20). Meanwhile, heat is consumed by the convective heat transfer,  $\dot{Q}_{conv}$ , due to the cooled lye flow entering the electrolyzers. Heat is also consumed by the surroundings of the electrolyzers, namely the conductive heat transfer,  $\dot{Q}_{cond}$ . As a result, the energy balance can be extended as follows:

$$C_t \frac{dT^{el,j}}{dt} = \underbrace{n_c (U - U_{tn})}_{\dot{Q}_{loss}} - \underbrace{\dot{m}_{lye,in}^{el,j} C_{p_{lye}} (T^{el,j} - T_{in}^{el,j})}_{\dot{Q}_{conv}} - \underbrace{A_s \left[ h_c (T^{el,j} - T_a) + \sigma \epsilon (T^{el,j,4} - T_a^4) \right]}_{\dot{Q}_{cond}}, \quad (2.20)$$

where  $\dot{m}_{lye,in}^{el,j}$  is the mass entering the electrolyzer,  $C_t$  is the overall thermal capacity and  $C_{p_{lye}}$  is the heat capacity of the lye. Further,  $n_c$  is the number of cells for one stack, while  $U$  is the voltage.  $A_s$  is defined as the active area of the electrolytes,  $h_c$  is related to convective heat transfer and  $T_a$  is the ambient temperature surrounding the electrolyzers. Lastly,  $\sigma$  represents Stefan-Boltzmann's

constant set to  $5.6704 \cdot 10^{-8} \text{W/m}^2\text{K}^4$ , and  $\epsilon$  represents the dimensionless emissivity constant set to 0.8.

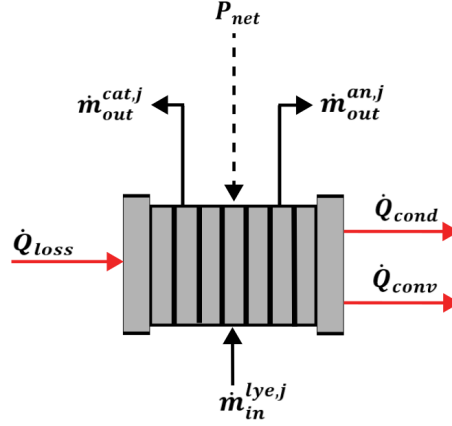


**Figure 2.3:** Inputs and outputs for one electrolyzer. The power input is  $P_{net}$  illustrated with a dashed line, while mass flows are represented with black lines and the heat transfer with red lines. The electrolyzer drawing is inspired by Lucas Cammann[2] and designed in Inkscape[3].

## 2.2.2 Separators

To separate the product gases with the recycled liquid lye, gas-liquid separators are included for each electrode. Hence, as for the electrolyse equations,  $j$  denotes the separators at electrolyzer 1, 2 and 3. At the anodic separator the gas phase mainly consist of oxygen, while the gas phase at the cathodic separators mainly contain hydrogen. A sketch of the anodic separator is presented in Figure 2.4. Due to the assumption of the separation process being adiabatic, no energy balance is needed. Meanwhile, the overall mass balances for the anodic and cathodic separators are defined as follows:

$$\begin{aligned} \frac{dm^{sep,an,j}}{dt} &= \sum \dot{m}_{in}^j - \sum \dot{m}_{out}^j \\ &= M_{H_2} \left( \dot{n}_{out,H_2}^{an,j} - \dot{n}_{out,H_2}^{sep,an,j} \right) \\ &\quad + M_{O_2} \left( \dot{n}_{out,O_2}^{an,j} - \dot{n}_{out,O_2}^{sep,an,j} - \dot{n}_{in,O_2}^{buffer,j} \right) \\ &\quad + 0.5 \dot{m}_{lye,out}^{el,j} - 0.5 \dot{m}_{lye,in}^{buffer,j} \end{aligned} \quad (2.21)$$

$$\begin{aligned} \frac{dm^{sep,cat,j}}{dt} &= \sum \dot{m}_{in}^j - \sum \dot{m}_{out}^j \\ &= M_{O_2} \left( \dot{n}_{out,O_2}^{cat,j} - \dot{n}_{out,O_2}^{sep,cat,j} \right) \\ &\quad + M_{H_2} \left( \dot{n}_{out,H_2}^{cat,j} - \dot{n}_{out,H_2}^{sep,cat,j} - \dot{n}_{in,H_2}^{buffer,j} \right) \\ &\quad + 0.5 \cdot \dot{m}_{lye,out}^{el,j} - 0.5 \cdot \dot{m}_{lye,in}^{buffer,j}, \end{aligned} \quad (2.22)$$

assuming that half of the lye stream constitutes of the anodic lye, while the other half of the cathodic lye form the separators. The molar component balances for hydrogen and oxygen is defined as:

$$\begin{aligned}\frac{dn_{H_2}^{sep,an,j}}{dt} &= \dot{n}_{out,H_2}^{an,j} - \dot{n}_{out,H_2}^{sep,an,j} \\ \frac{dn_{O_2}^{sep,an,j}}{dt} &= \dot{n}_{out,O_2}^{an,j} - \dot{n}_{out,O_2}^{sep,an,j} - \dot{n}_{in,O_2}^{buffer,j} \\ &= \dot{n}_{out,O_2}^{an,j} - \dot{n}_{out,O_2}^{sep,an,j} - 0.5 \cdot \frac{\dot{m}_{lye,in}^j S_{O_2,lye} P_{sys}}{\rho_{lye} \eta_{sep}}\end{aligned}\quad (2.23)$$

$$\begin{aligned}\frac{dn_{O_2}^{sep,cat,j}}{dt} &= \dot{n}_{out,O_2}^{cat,j} - \dot{n}_{out,O_2}^{sep,cat,j} \\ \frac{dn_{H_2}^{sep,cat,j}}{dt} &= \dot{n}_{out,H_2}^{cat,j} - \dot{n}_{out,H_2}^{sep,cat,j} - \dot{n}_{in,H_2}^{buffer,j} \\ &= \dot{n}_{out,H_2}^{cat,j} - \dot{n}_{out,H_2}^{sep,cat,j} - 0.5 \cdot \frac{\dot{m}_{lye,in}^j S_{H_2,lye} P_{sys}}{\rho_{lye} \eta_{sep}},\end{aligned}\quad (2.24)$$

where  $\rho_{lye}$  is the lye liquid density,  $\eta_{sep}$  is the efficiency and the solubility  $S_{i,lye}$  for component  $i$  is defined as:

$$\begin{aligned}S_{i,lye} &= \frac{S_{i,H_2O}}{10^{K_i w_{lye}}}, \text{ where} \\ S_{i,H_2O} &= \frac{\rho_{H_2O}}{M_{H_2O} P_{atm} H_{i,H_2O}}.\end{aligned}\quad (2.25)$$

$w_{lye}$  denotes the mass fraction of the lye set to 0.312, the included  $K_i$  is the Setchenov constant set to 3.14 and  $H_i$  is Henry's solubility set to  $7.1698 \cdot 10^4 atm^{-1}$ [19].

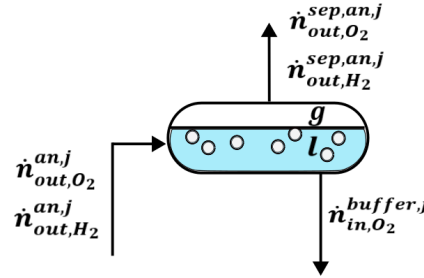


**Figure 2.4:** Liquid-gas separator at the anodic electrode.  $\dot{n}_i$  is the molar flow of component  $i$ .  $g$  and  $l$  denote gas and liquid phase respectively. The drawing is inspired by Lucas Cammann[2] and designed in Inkscape[3].

### 2.2.3 Buffer tank

The liquid flows from the six separators is mixed with the make-up water flow in the buffer tank, see Figure 2.1. Thus, the overall mass balance and the associated component balance is modeled

as:

$$\begin{aligned} \frac{dm^{buffer}}{dt} &= \sum_j \dot{m}_{lye,in}^{buffer,j} + \dot{m}_{lye,makeup} - \sum_j \dot{m}_{lye,in}^{el,j} \\ &+ M_{H_2} \cdot \sum_j \left( \dot{n}_{in,H_2}^{buffer,j} - 2\dot{n}_{in,H_2}^j \right) + M_{O_2} \cdot \sum_j \left( \dot{n}_{in,O_2}^{buffer,j} - 2\dot{n}_{in,O_2}^j \right) \end{aligned} \quad (2.26)$$

$$\begin{aligned} \frac{dn_{H_2}^{buffer}}{dt} &= \sum_j \dot{n}_{in,H_2}^{buffer,j} - 2 \cdot \sum_j \dot{n}_{in,H_2}^j \\ \frac{dn_{O_2}^{buffer}}{dt} &= \sum_j \dot{n}_{in,O_2}^{buffer,j} - 2 \cdot \sum_j \dot{n}_{in,O_2}^j, \end{aligned} \quad (2.27)$$

where  $j$  denotes electrolyzer 1, 2 and 3. The following energy balance is simplified as:

$$\begin{aligned} \frac{dU}{dt} &= \sum \dot{Q}_{in} - \sum \dot{Q}_{out} \\ \frac{dm^{buff}}{dt} C_{p_{lye}} T^{buff} + m^{buff} C_{p_{lye}} \frac{dT^{buff}}{dt} &= \sum_j \dot{m}_{lye,in}^{buffer,j} \cdot C_{p_{lye}} \left( T_{avg}^{el} - T_0 \right) \\ &+ \dot{m}_{makeup,H_2O} \cdot C_{p_{H_2O}} (T_{in,H_2O} - T_0) \\ &- \sum_j \dot{m}_{lye,in}^{el,j} \cdot C_{p_{lye}} \left( T^{buff} - T_0 \right), \end{aligned} \quad (2.28)$$

where  $T_0$  is set to 273 K, and  $T_{avg}^{el}$  is the average temperature for each electrolyzer  $j$ .

### 2.2.4 Heat exchangers

As presented in Figure 2.1, there are three heat exchangers. The heat exchangers are modeled as counter-current exchangers with the quantitative temperature profiles presented in Figure 2.5. The mass balances of the heat exchangers are neglected as it is assumed to be perfectly controlled. Meanwhile, the energy balance for the heat exchanger at electrolyzer  $j$  is presented as:

$$m_{lye}^{HX,j} \frac{dT_{in}^{el,j}}{dt} = \dot{m}_{lye,in}^{el,j} \cdot C_{p_{lye}} \left( T^{buff} - T_{in}^{el,j} \right) + U A_{HX} \Delta T_{LMTD,j} \quad (2.29)$$

$$m_{cw}^{HX,j} \frac{dT_{cw,out}^j}{dt} = \dot{m}_{cw}^{el,j} \cdot C_{p_{lye}} \left( T_{cw,in} - T_{cw,out}^j \right) + U A_{HX} \Delta T_{LMTD,j}. \quad (2.30)$$

Due to numerical difficulties, the logarithmic temperature difference,  $T_{LMTD}$ , is defined as:

$$\Delta T_{LMTD,j} = \frac{T^{buff} + T_{in}^{el,j}}{2} - \frac{T_{cw,out}^j + T_{cw,in}}{2}. \quad (2.31)$$

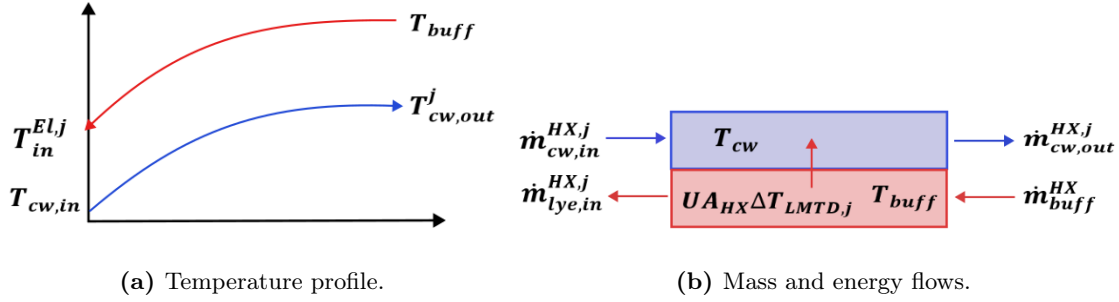


**Figure 2.5:** Heat exchanger temperature profile and energy and mass flows. The drawing is inspired by Lucas Cammann[2] and designed in Inkscape[3].

### 2.2.5 Compressor duty

The product outflows of each separator are compressed into the storage tanks, see Figure 2.1. Hence, the compressor duty for component  $i$  is set as[20]:

$$W_{comp} = \frac{\dot{n}_{out,i}^{sep} RT \kappa}{\eta_{comp} (\kappa - 1)} \cdot \left[ \left( \frac{P_{sto,i}}{P_{sys}} \right)^{\kappa-1/\kappa} - 1 \right], \quad (2.32)$$

where the storage pressure,  $P_{sto,i}$ , is assumed to be 25 bar and the heat capacity ratio,  $\kappa$ , is set to 1.4 for both  $H_2$  and  $O_2$ . Additionally,  $\eta_{comp}$  is the compressor efficiency, which is set to 0.8 for this model[2].

## 2.3 Wind turbine power

In order to produce green hydrogen, the energy source is essential. To avoid emitting greenhouse gases, fossil fuels are abandoned and renewable alternatives are considered. For this model, the hydrogen plant will be operated using wind power. This is a technology which has proven to hold large benefits with considerable efficiencies at 40–50%[21]. Through turbines, or blades, the kinetic energy from the wind velocity is converted into mechanical energy, which is further transformed to electrical energy[22]. It should be mentioned that there are limitations for utilizing the power generated by the turbine park. This includes the AC/DC converter that is required for power supplies[8]. However, these limitations are not included in this project, assuming that 100% of the generated power,  $P_{net}$ , is supplied to the plant.

### 2.3.1 Weibull distribution

To be able to describe the wind variations for a given location, it is common to present the wind velocity or power data through the Weibull distribution[23]. Weibull distribution is a continuous probability distribution function with a scale parameter  $\lambda$  and a shape parameter  $k$ :

$$f(x; \lambda; k) = \begin{cases} \frac{k}{\lambda} \left( \frac{x}{\lambda} \right)^{k-1} e^{-(x/\lambda)^k}, & x \geq 0, \\ 0, & x < 0. \end{cases} \quad (2.33)$$

For a given set of data with wind velocity  $v$  [m/s], the scale ( $\lambda$ ) and shape ( $k$ ) parameter can be estimated through the mean velocity,  $v_m$ , and the standard derivation,  $\gamma$ :

$$k = \left( \frac{\gamma}{v_m} \right)^{-1.086} \quad (2.34)$$

$$\lambda = \frac{v_m}{\Gamma(1 + 1/k)}. \quad (2.35)$$

The Gamma distribution function is defined as  $\Gamma[x] = \int_0^\infty u^{x-1} e^{-u} du$ [23].

Though the Weibull distribution, the weighted production rate of green hydrogen can be found through:

$$\bar{n}_{H_2,out} = f(v; \lambda; k) \cdot \dot{n}_{H_2,out} \quad (2.36)$$

where  $\dot{n}_{H_2,out}$  is the absolute production rate. Thus, the weighted production rate constitutes of the absolute production rate given the probability of the occurrence of a specific wind velocity.

### 2.3.2 The present value method

To evaluate the profitability of a given project, the net present value (NPV) and internal rate of return (IRR) are commonly used methods. For mutually exclusive projects, where only one project can be chosen, IRR can lead to inconclusive evaluations. Thus, assuming mutually exclusive projects, NPV should be used[24]. NPV is today's value of future cash flows minus the investment at the start of the project[25]:

$$NPV = -C_0 + \sum_y \frac{CF}{(1+r)^y}, \quad (2.37)$$

where  $y$  is years,  $r$  is the cost of capital and  $C_0$  is the investment cost in year 0, and  $CF$  is the future cash flows. The cost of capital depends on the capital structure of the company making the investment. For the project to be profitable, the NPV must be positive. Hence, the profitability of the project also relies on the cost of capital for the company investing.

## Method and Model Implementation

The model of the green hydrogen plant is implemented using *Julia*[26], see Appendix A.2. The model is based on the code by Lucas Cammann and further modified for a larger-scale plant with three electrolyzers[27]. The simulation is further performed both without and with bubble formation, where the limiting current density is set to  $7500 \text{ A m}^{-1}$ , see equation (2.12). Additionally, different performance parameters are set for the three electrolyzers to illustrate the effect of degradation, see Appendix A.1. Since electrolyzer 1 is modeled with the most efficient performance parameters, it is at the start of its lifespan. Meanwhile, electrolyzer 2 and 3 are modeled with degraded performance parameters, with electrolyzer 3 being close to the end of its lifespan. Realistic wind data from renewables.ninja is also utilized to examine the behavior of the simulated plant[1].

### 3.1 Optimization setup

To obtain the optimal production of hydrogen gas,  $\dot{n}_{out,H_2}$ , for fluctuating power inputs,  $P_{net}$ , a nonlinear optimization problem, NLP, is formalized by Lucas Cammann [2]. The optimization problem aims to maximize the production of hydrogen gas within sufficient constraints. These constraints are set to ensure the feasible and safe operation of the plant. To solve the optimization problem, *Ipopt* (Interior Point Optimizer) is used[28]. *Ipopt* is an open-source software package, which solves NLP's on the following form:

$$\begin{aligned}
 \min_u \quad & h(u, x, d) \\
 \text{s.t.} \quad & f(u, x, d) = 0 \\
 & g(u, x, d) \leq 0
 \end{aligned} \tag{3.1}$$

where  $h(u, x, d)$  is the cost function, which is set as the total output of hydrogen gas. Additionally,  $f(u, x, d)$  are set as the model equations, while  $g(u, x, d)$  are set as the constraints. Further,  $x$  is



the state variables,  $u$  is the manipulated variables and  $d$  is the disturbance:

$$\begin{aligned}
x &= [T_{buff}, I, \dot{n}_{in,H_2}^j, \dot{n}_{in,O_2}^j, \dot{n}_{out,H_2}^{cat,j}, \dot{n}_{out,H_2}^{an,j}, \dot{n}_{out,O_2}^{cat,j}, \dot{n}_{out,O_2}^{an,j}, \dot{n}_{out,H_2}^{sep,an,j}, \dot{n}_{out,O_2}^{sep,an,j}, \\
&\quad \dot{n}_{out,H_2}^{sep,cat,j}, \dot{n}_{out,O_2}^{sep,cat,j}, T_i^{El,j}, T_o^{cw,j}, m_{lye,out}^{el,j}, m_{lye,in}^{buffer}, \dot{m}_{lye,makeup}, \theta] \\
u &= [U, T^{El,j}, P_{sys}, m_{cw}^{el,j}, \dot{m}_{lye,in}^{el,j}] \\
d &= [P_{net}]
\end{aligned} \tag{3.2}$$

Thus, when operating with flexible constraints for each electrolyzer,  $j$ , the degrees of freedom is 11. Consequently, the NLP for maximum hydrogen production is found using the following formulation[2]:

$$\begin{aligned}
\max \quad & \dot{n}_{out,H_2} \\
\text{s.t.} \quad & 1 \text{ kg s}^{-1} \leq \dot{m}_{lye,k}^{d,j} \leq 30 \text{ kg s}^{-1} \quad \forall k \text{ in } [in, out], d \in [el, buff] \\
& \dot{m}_{cw}^j \leq 26.6 \text{ kg s}^{-1} \\
& 10^\circ\text{C} \leq T^{el,j} \leq 80^\circ\text{C} \\
& -20^\circ\text{C} \leq \Delta T_{in}^{el,j} \leq 20^\circ\text{C} \\
& \text{HTO}^j \leq 2\% \\
& \sum_j P_{comp}^j + \sum_j P_{el}^j \leq P_{net} \\
& 2 \text{ bar} \leq P_{sys} \leq 25 \text{ bar}
\end{aligned} \tag{3.3}$$

To maintain a safe HTO level, the upper limit is set to not exceed 2 *vol.*%, as discussed in section 2.1.1. Likewise, the required power consumption can not exceed the power input,  $P_{net}$ , supplied by the wind turbine park. The flow rates, pressure, and temperature constraints are set according to Georgios Sakas [18] and Lucas Cammann[2]. The above equation (3.3) yields flexible setpoints for the pressure and the lye flowrate. Meanwhile, fixed setpoints for the pressure and the lye flowrate are also optimized for, with the minimal setpoints formulated as:

$$\begin{aligned}
0.99 \text{ kg s}^{-1} &\leq \dot{m}_{lye,k}^{d,j} \leq 1.01 \text{ kg s}^{-1} \quad \forall k \text{ in } [in, out], d \in [el, buff] \\
1.98 \text{ bar} &\leq P_{sys} \leq 2.02 \text{ bar},
\end{aligned} \tag{3.4}$$

an maximal setpoints formulated as:

$$\begin{aligned}
29.7 \text{ kg s}^{-1} &\leq \dot{m}_{lye,k}^{d,j} \leq 30.3 \text{ kg s}^{-1} \quad \forall k \text{ in } [in, out], d \in [el, buff] \\
24.75 \text{ bar} &\leq P_{sys} \leq 25.25 \text{ bar}.
\end{aligned} \tag{3.5}$$

## 3.2 Wind turbine data

Realistic wind data for the model is found through the website renewables.ninja[1]. The website provides hourly power output from solar and wind parks, which is estimated by analyzing weather reports and satellite signals from any location in the world. The location used for this model is set

according to an article by Ragnar Lurås [29], where Hovde in Opdalen is proposed as a suitable location, see Figure 3.1. Hovde is currently considered as a location for installing wind turbines, which will supply the industrial park at Herøya in Porsgrunn with renewable energy in the near future. Additionally, Yara is currently developing Norway’s first green hydrogen plant at Herøya according to *Offshore Energy* by Pekic[30]. Thus, Hovde is selected as a reasonable location for collecting hourly wind data containing both power output and wind velocities.

The wind capacity is also set in order to simulate the power outputs at Hovde. Based on the article by Vogt [31], the power capacity is the power generated with optimal wind conditions for a given turbine. Thus, using the nominal power at approximately 2 MW for a single stack, the wind park is simulated with capacities at 5 MW, 6 MW and 7 MW[31].



**Figure 3.1:** The map of Porsgrunn and Hovde is found from renewables.ninja[1] and edited in Inkscape[3].

### 3.2.1 Profitability estimation

To evaluate the profitability of operating with different capacities, the net present value is used, see section 2.3.2. It should be emphasized that the calculations done in this project are based on estimates. Regardless, the results can be used as an indication of whether larger capacities yield greater profitability. Only the installation of the wind turbines are considered as the installation of the plant is assumed to be the same for all capacities. The investment cost is found to be \$1.3 million per MW of capacity according to Blewett [32], and the price of hydrogen is currently \$3.70/kg according to Morgan [33]. Meanwhile, the unlevered cost of capital is found to be 6,5% for onshore wind reported by Freyman [34]. Finally, the project lifetime is set to 15 years.

## Results and Discussion

The results of the modeled green hydrogen plant are presented below. To validate the model, both with and without bubble formation, the active constraint regions are analyzed. Further, the performance parameters for each electrolyzer are discussed. The simulated wind data from renewables.ninja is also processed and utilized to evaluate different setpoints and capacities for production in 2019.[1] Finally, an estimate of the profitability is presented for each of the simulated wind capacities.

### 4.1 Active constraint regions

The active constraint regions are analyzed by solving the NLP presented in equation (3.3) with a power input ranging from 0.03 MW to 6.5 MW. The constraints are active if, for a given power input, the variable is at the maximal or minimal setpoint. Figure 4.1 presents the plant behavior without bubble formation. To analyze the plot, three regions are evaluated. The first region ranges from 0.03 MW to 1 MW. As a result of the low power inputs, the current density is limited, forcing the HTO to its maximal constraint. In order to counteract the HTO level, the lye flowrate is expected to stay at its minimal constraints. Despite this, the lye flowrate suddenly rises before reaching its minimal constraint. This may be a result of the limited heat generation in the electrolyzer, caused by the low current densities. As mentioned in section 2.1.1, heat is required to operate at cell voltages below the thermoneutral cell voltage at  $U_{tn} = 1.482$  V. The cell voltage is therefore found to reach this thermoneutral cell voltage at a power input at approximately 0.4 MW. Hence, the lye flowrate is increased in order to add heat to the electrolyzer. For the same reason, the temperatures are also increased in this region. The pressure, however, rises with greater current densities as the HTO decreases. This is done to gain more efficient production.

The second region ranges from 1 MW to 4 MW, where the HTO level is significantly decreased due to the increased current densities. Meanwhile, the pressure remains at its maximal constraint in order to obtain efficient production and prevent extra power costs for the compressors. The lye flowrate is operated close to its minimal constraint[2].

The third, and last, region ranges from 4 MW to 6.5 MW. In this region, the cooling water is

rised in order to keep the temperature in the electrolyzers within its maximal constraint at  $80^\circ\text{C}$ . Consequently, the lye flowrate also rise to its maximal constraint, which initially would lead to an increase in the HTO level. However, due to the increased current densities in this region, the HTO level is not affected. In fact, the HTO level decreases as the pressure reaches its minimal constraint. Operating at minimal pressure increases the compressor costs, but since the power input is increased, the compressor is supplied with enough power to decrease the pressure of the system. There is also a spike in the HTO at approximately 4.5 MW. However, this could be caused by the sudden increase in the lye flowrate.

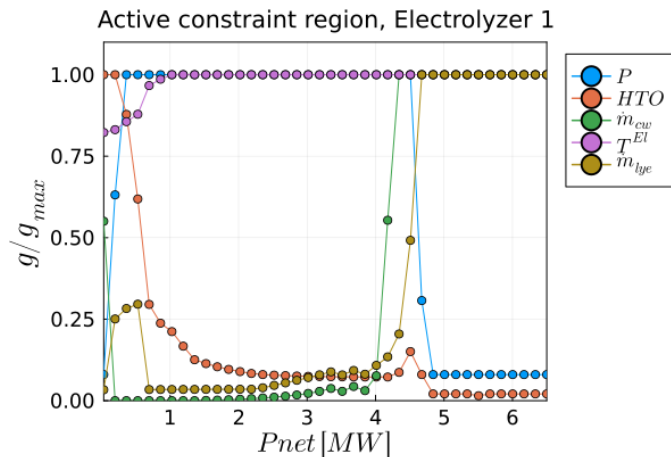


**Figure 4.1:** Active constraint regions for electrolyzer 1 without bubble formation. The power input,  $P_{net}$  ranges from 0.03 MW to 6.5 MW. The circles mark the solution to the NLP in equation (3.3).  $g/g_{max}$  is the ratio of the solution for the current power input,  $g$ , and the maximal setpoint,  $g_{max}$ [2].

The active constraint regions presented in Figure 4.2 are modeled with bubble formation. Similarly as for the previous model, the plot is separated into three regions, where the first region range from 0.03 MW to approximately 1.6 MW. Compared to the model without bubbles, the lye flowrate is set to its maximal constraint in order to counteract the bubble formation. This leads to the HTO level staying at its maximal constraint throughout the first region. Meanwhile, the temperature and pressure are both risen to their maximal constraints, and the cooling water is kept at its minimal constraint.

In the second region, ranging from 1.6 MW to 4.4 MW, the HTO level is finally decreased despite the lye flowrate remaining at its maximal constraint. As for the model without bubble formation, this is due to increased current densities. Thus, a further decrease in the HTO level is achieved in the third region, ranging from 4.4 MW to 6.5 MW. In addition to the increased current densities, this is also caused by the pressure reaching its minimal constraint at 5 MW. Lastly, the cooling water increase to its maximal constraint in order to keep a feasible operating temperature[2].

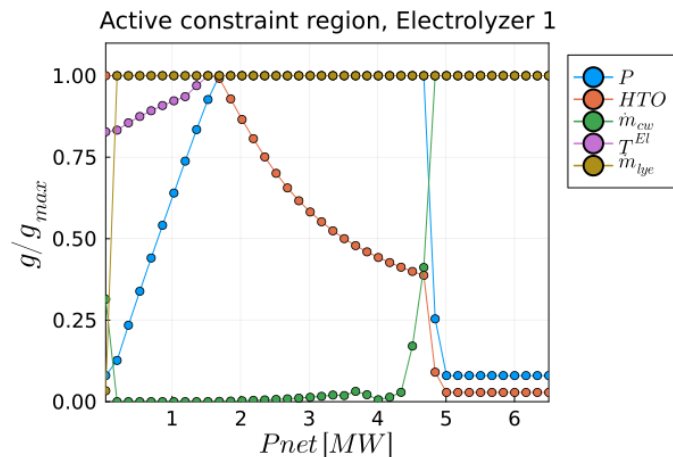


**Figure 4.2:** Active constraint regions for electrolyzer 1 with bubble formation. The power input,  $P_{net}$  ranges from 0.03 MW to 6.5 MW. The circles mark the solution to the NLP in equation (3.3).  $g/g_{max}$  is the ratio of the solution for the current power input,  $g$ , and the maximal setpoint,  $g_{max}$ [2].

## 4.2 Performance parameters

Different performance parameters are implemented in order to illustrate how degradation affects the electrolyzers, see Appendix A.1. Electrolyzer 1 is set as the most efficient, while the efficiency for electrolyzers 2 and 3 are decreased and therefore degraded. Hence, the NLP presented in equation (3.3) yields different results for the active constraint regions. First, the model without bubble formation is presented in Figure 4.3 for electrolyzers 2 and 3 respectively. For both electrolyzers, the lye flowrate rises within the range of 0 to 2 MW. Compared with electrolyzer 1, however, this rise occurs at larger power inputs. This could be explained by the degenerated electrolyzers generating less heat at lower current densities, see equation (2.8). Additionally, at power inputs between 3 and 4 MW, the cooling water of the degraded electrolyzers both rises before experiencing a dip and then increasing to the maximal constraint. Similar behavior is found for the model with bubble formation, see Figure 4.4. This behavior is unexpected and could be due to a numerical error in the model which should be investigated further.

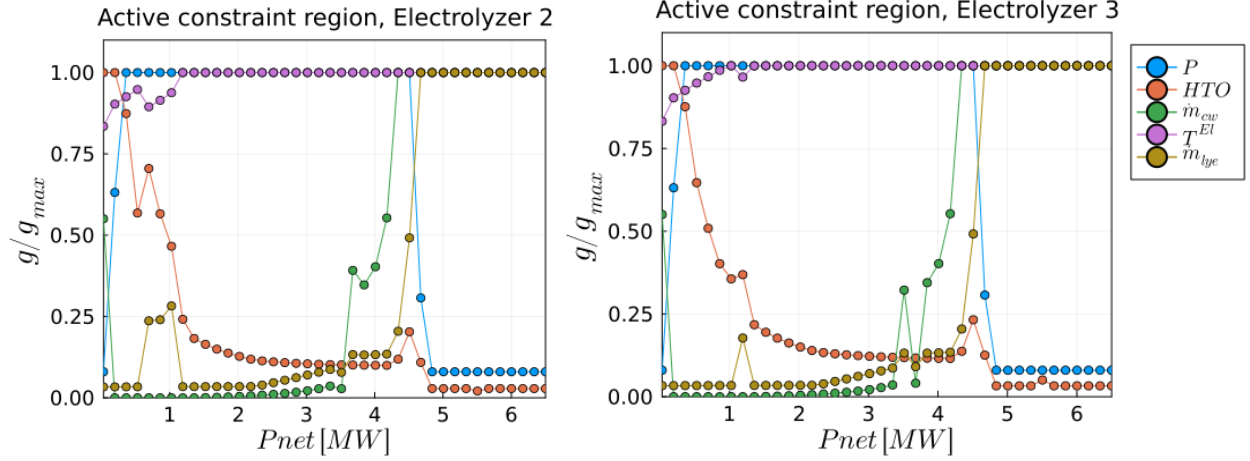


**Figure 4.3:** Active constraint regions for electrolyzer 2 and 3 without bubble formation. The power input,  $P_{net}$  ranges from 0.03 MW to 6.5 MW. The circles mark the solution to the NLP in equation (3.3).  $g/g_{max}$  is the ratio of the solution for the current power input,  $g$ , and the maximal setpoint,  $g_{max}$ [2].

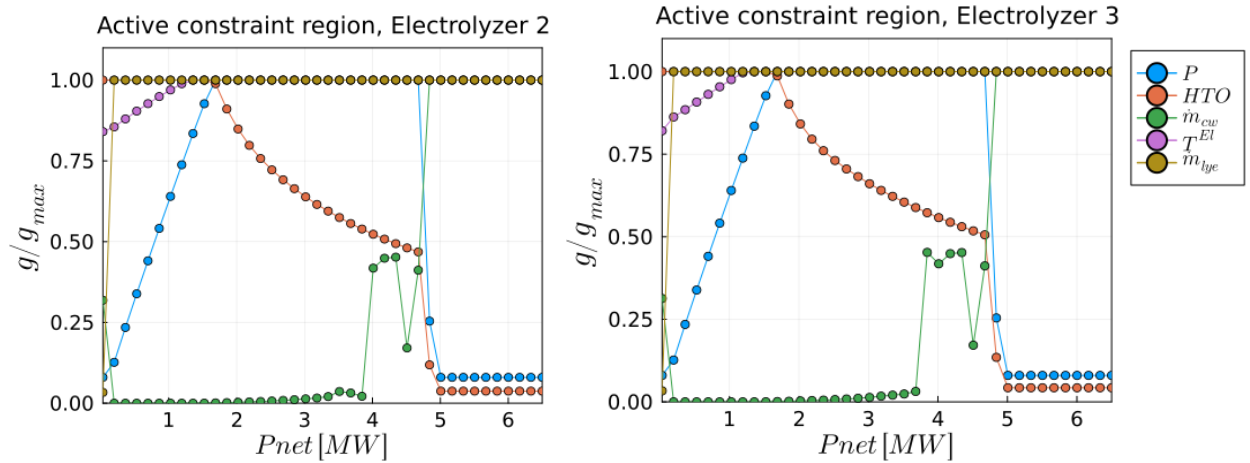


**Figure 4.4:** Active constraint regions for electrolyzer 2 and 3 with bubble formation. The power input,  $P_{net}$  ranges from 0.03 MW to 6.5 MW. The circles mark the solution to the NLP in equation (3.3).  $g/g_{max}$  is the ratio of the solution for the current power input,  $g$ , and the maximal setpoint,  $g_{max}$ [2].

#### 4.2.1 Bubble formation

The formation of bubbles is presented in Figure 4.5 for each of the three electrolyzers  $\theta[j]$ . For all of the electrolyzers, the bubble formation increases with greater power inputs. This is due to increasing power resulting in greater current densities and bubble formation according to equation (2.10). The bubble formation also reaches its maximum as the current density limit is reached at approximately 4.8 MW. Considering the three electrolyzers,  $\theta[j]$ , the bubble formation increases with greater efficiencies, as greater efficiency yields greater current densities. Additionally, an

unexplained change in the bubble formation occurs at approximately 1.2 MW. This is unexpected and should be researched further.

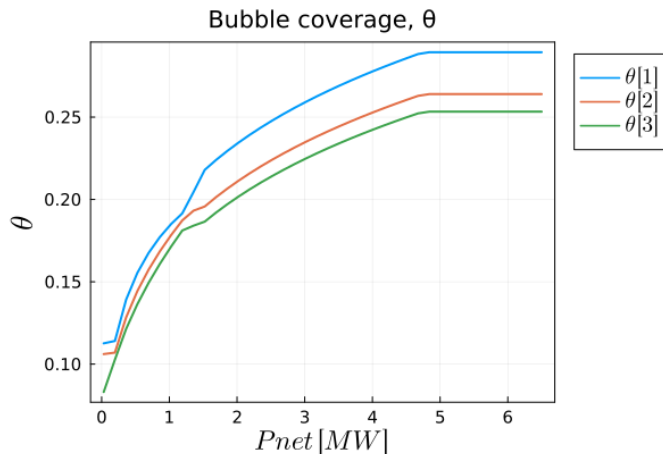


**Figure 4.5:** Bubble formation for each electrolyzer,  $\theta[j]$ , with power input,  $P_{net}$ , ranging from 0.03 MW to 6.5 MW.

### 4.3 Weibull distribution

As explained in section 3.2, wind data is simulated at Hovde in Opdalen using renewables.ninja[1]. Figure 4.6 presents the weekly average power outputs for 2019, with a capacity at 6 MW. The plot illustrates the varying power generated through the year, ranging from 0.013 MW to 5.477 MW. These variations pose challenges compared to conventional hydrogen production, using natural gas as fuel.

The data is further evaluated through Weibull distribution for 6 MW, see Figure 4.7. According to the distribution, the curve flattens with increased powers. As a result, larger power generations are rare while intermediate wind velocities occur more frequently. Additionally, the average generated power is found by locating the global maximum at approximately 1.182 MW. This average is significantly low compared to the nominal power demand of the plant at 6 MW. A solution to this difference in the average power generation and nominal power demand could be to simulate for greater capacities or consider a different location.

The Weibull distribution curves for 5 MW and 7 MW are included in Figure 4.8, and 4.9 respectively. The shape of the distribution curves is similar to the capacity of 5 MW, but have an average power generation at 0.985 MW for capacity at 5 MW, and 1.379 MW for capacity at 7 MW.

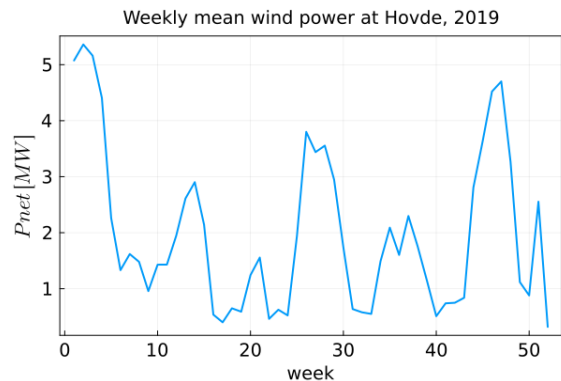


**Figure 4.6:** Weekly mean of the generated wind power at Hovde in 2019. The capacity for the simulation is set to 6 MW, and simulated using *renewables.ninja*[1].

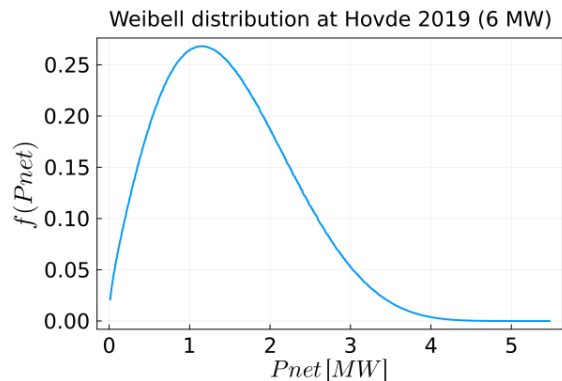


**Figure 4.7:** The weibull distribution for the simulated wind power at Hovde in 2019 with capacity at 6 MW. The weibull function,  $f$ , is presented in (2.33).

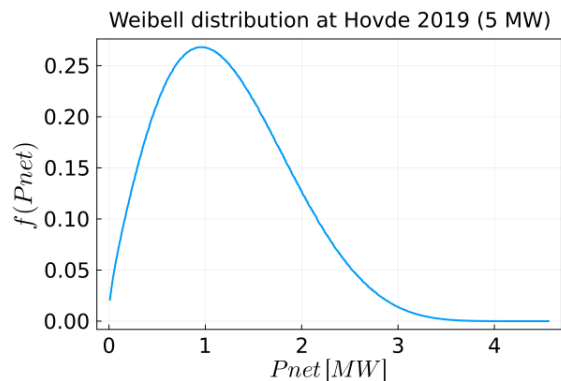


**Figure 4.8:** The weibull distribution for the simulated wind power at Hovde in 2019 with capacity at 5 MW.

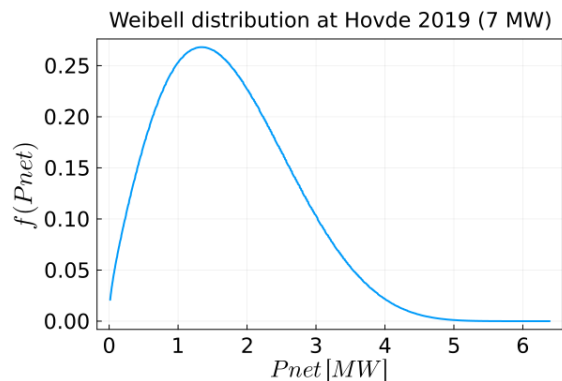


**Figure 4.9:** The weibull distribution for the simulated wind power at Hovde in 2019 with capacity at 7 MW.

## 4.4 Flexible and fixed constraints

The simulated wind data is utilized to analyze the operation with minimal, maximal and flexible setpoints. Both the absolute and weighted production rate is evaluated by implementing the power inputs with capacities at 5 MW, 6 MW, and 7 MW. Accordingly, the downtime is also documented for each capacity.

The absolute and weighted production rates for the different setpoint combinations are presented in Figure 4.10 with a capacity of 6 MW. As illustrated, at low power inputs, until approximately 1.6 MW, operation with minimal and flexible setpoints yields relatively similar absolute and weighted production rates. Operating with maximal setpoints, however, yields no production with downtime of 7417 h, see Table 4.1. This behavior is expected as lower power inputs result in high HTO levels. To keep the HTO within its feasible constraints, low pressure and flowrates are required. Thus,



operating with maximal setpoints leads to infeasible operation for the HTO level which further forces plant shutdown. Additionally, with low power inputs comes low current densities which result in less bubble formation. High lye flowrates are therefore not needed to counteract bubble formation. Low pressure is also efficient, as lower gas production requires less compression power. After reaching a power input at 1.6 MW operation with minimal setpoints results in a constant absolute production rate and a decrease in weighted production rate. Meanwhile, operating with maximal setpoints results in the same absolute and weighted production rate as operating with flexible setpoints. This is also expected, as larger power inputs yield lower HTO levels, allowing the pressure and the lye flowrates to increase. Operating with maximal pressure reduces the compression duty, while maximal lye flowrate counteracts the bubble formation which increases the production rate.

Operations with wind capacities at 5 MW and 7 MW result in the same absolute and weighted production rate profiles, see Figure 4.11 and 4.12 respectively. However, larger capacities lead to greater integrated absolute and weighted production rates, see Table 4.1. This is found by integrating the curves in Figures 4.11, 4.10, and 4.12 using trapezoidal integration. The total production through 2019 also increases with greater capacities as presented in Table 4.1. This is expected as larger power inputs increase the current densities, which further increases the production according to (2.16) and (2.18). In addition, greater capacities cause greater current densities which counteract HTO and lead to less downtime when operating at maximal setpoints, see Figure 4.13.

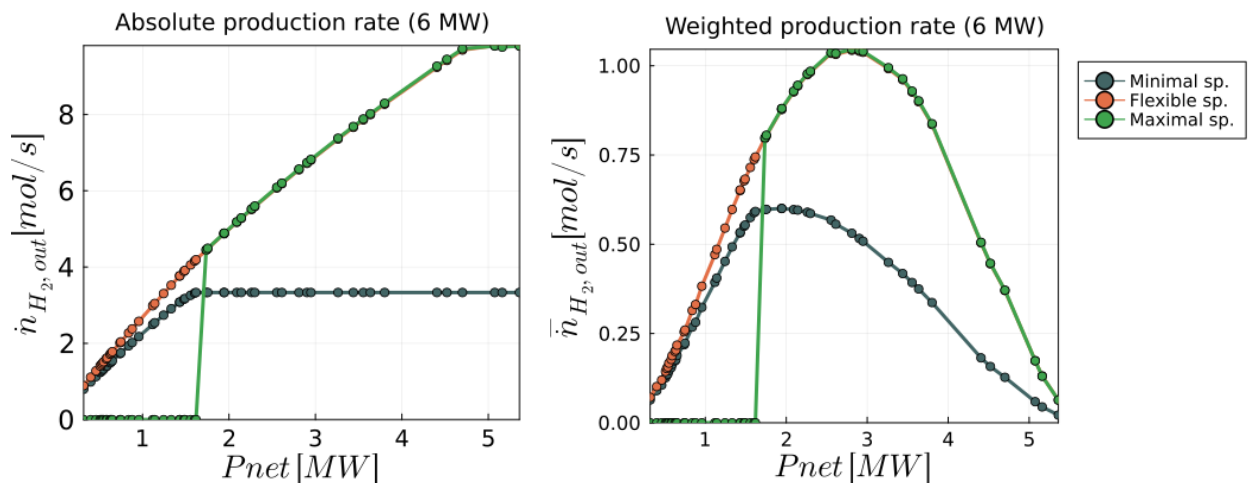


**Figure 4.10:** Absolute and weighted production rate for minimal, maximal, and flexible setpoints with a capacity of 6 MW.

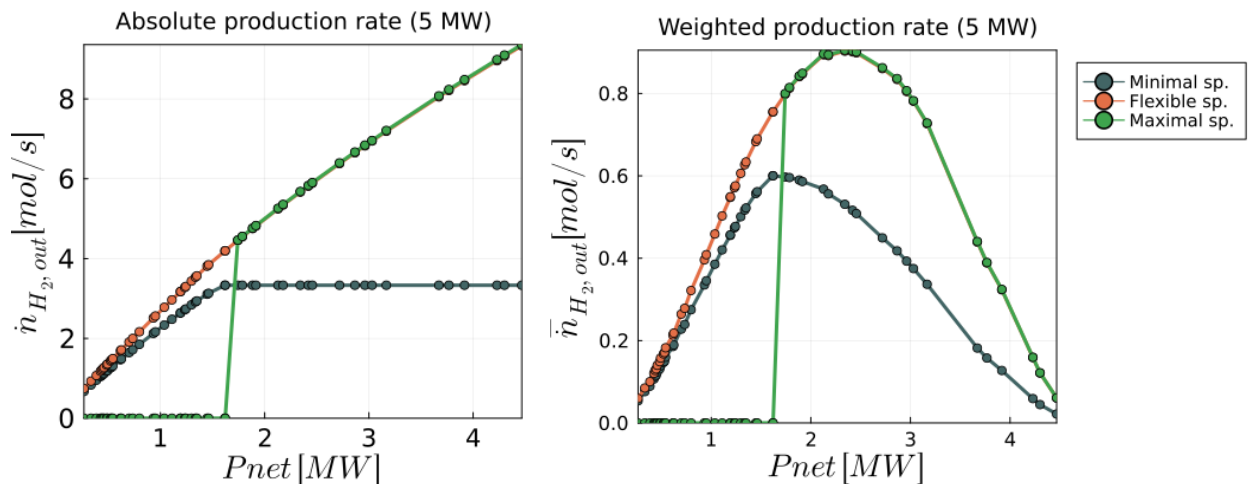


**Figure 4.11:** Absolute and weighted production rate for minimal, maximal, and flexible setpoints with a capacity of 5 MW.

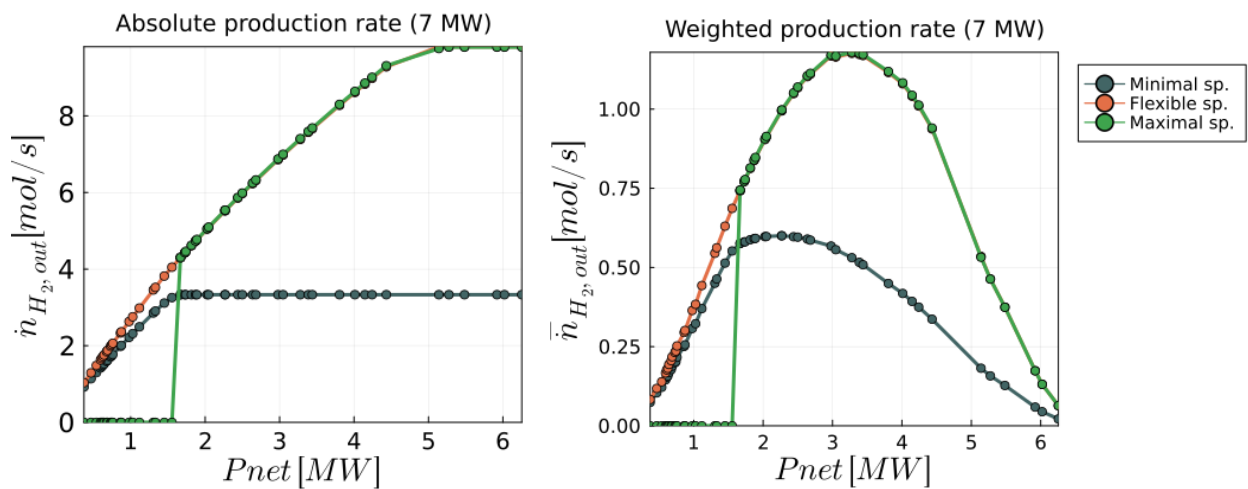


**Figure 4.12:** Absolute and weighted production rate for minimal, maximal, and flexible setpoints with a capacity of 7 MW.

**Table 4.1:** The integrated absolute and weighted production rate of hydrogen for operating at maximal, minimal, and flexible setpoints with capacities at 5 MW, 6 MW, and 7 MW. The total production of hydrogen through 2019 is also included.

Capacities	Operating setpoints:	Integrated	Integrated	Total production in 2019 [ton]
		absolute production rate [mol MW s <sup>-1</sup> ]	weighted production rate [mol MW s <sup>-1</sup> ]	
5 MW	Minimum	$1.235 \cdot 10^7$	$1.442 \cdot 10^6$	157.593
	Maximum	$1.944 \cdot 10^7$	$1.754 \cdot 10^6$	162.082
	Flexible	$2.306 \cdot 10^7$	$2.344 \cdot 10^6$	252.519
6 MW	Minimum	$1.529 \cdot 10^7$	$1.803 \cdot 10^6$	168.321
	Maximum	$2.813 \cdot 10^7$	$2.710 \cdot 10^6$	206.916
	Flexible	$3.169 \cdot 10^7$	$3.259 \cdot 10^6$	291.214
7 MW	Minimum	$1.882 \cdot 10^7$	$2.158 \cdot 10^6$	175.743
	Maximum	$3.707 \cdot 10^7$	$3.795 \cdot 10^6$	264.109
	Flexible	$4.032 \cdot 10^7$	$4.257 \cdot 10^6$	322.635

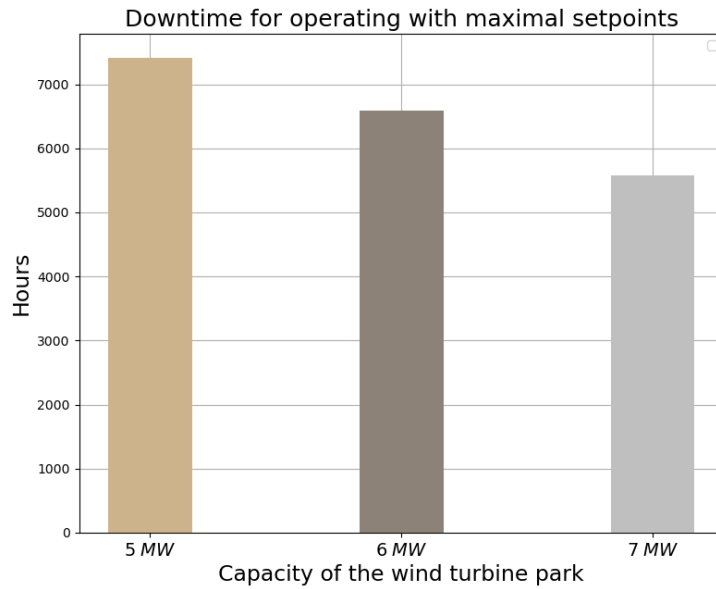


**Figure 4.13:** Downtime for production operating at maximal setpoints through 2019. 5, 6, and 7 MW yields 7117, 6594 and 5581 hours respectively.

## 4.5 Profitability estimation

Operating with larger capacities yields greater production rates as presented in Table 4.1. However, the installation of wind turbine parks with greater capacities also comes with larger investment

costs. Thus, the profitability of operation and installation at 5 MW, 6 MW, and 7 MW is evaluated through the net present value, see equation (2.37), with varying cost of capital, see Figure 4.14. Additionally, the cash flows are calculated for the total production in 2019 from Table 4.1, and assumed to be the same for each year. Thus, the most profitable capacity is found by analyzing Figure 4.14. As explained in section 3.2.1, the cost of capital is further assumed to be greater than 6.5% as this is the unlevered cost of capital for onshore wind power. Consequently, for cost of capital between 6.5% to 7.241% installation and operation with 6 MW are most profitable. Meanwhile, for cost of capital larger than 7.241%, installation and operation with 5 MW are most profitable.

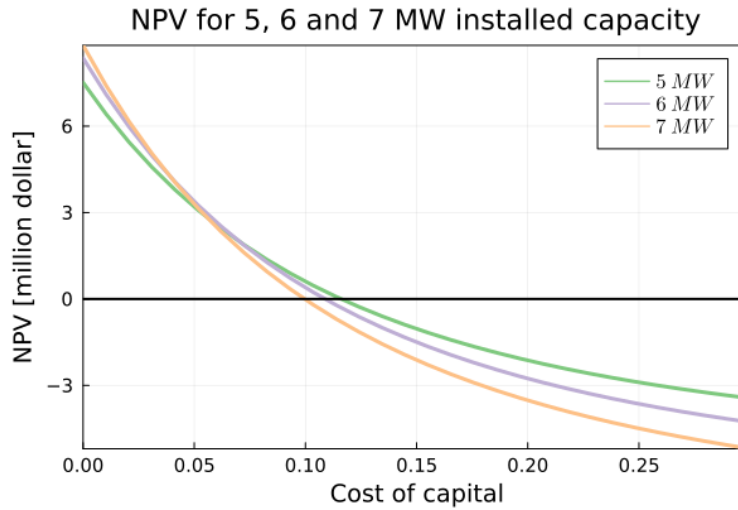


**Figure 4.14:** The present value profile for operation and investment at 5 MW, 6 MW, and 7 MW. The lifetime of the projects is set to 15 years.

## Conclusion and Further Research

This project has modeled and analyzed the optimal operating conditions with varying power inputs for a renewable hydrogen plant. The active constraint regions for both the model with and without bubble formation are analyzed in order to validate the model. An unexpected rise in the lye flowrate occurs at low power inputs for the model without bubble formation, see Figure 4.1. However, this could be caused by limited heat generation in the electrolyzers at low current densities. Thus, the lye flowrate is increased in order to compensate for the lack of heat. Meanwhile, the active constraint regions for the model with bubble formation are as expected, see Figure 4.2. The lye flowrate is increased to its maximal constraint for the entire range of power. This is done in order to counteract the bubble formation on the electrolyte surface. As a consequence, the HTO does not reach its minimal setpoint before 5 MW.

Further, the active constraint regions for the degraded electrolyzers are analyzed. For the model without bubble formation, the rise in the lye flowrate occurs at greater power inputs, see Figure 4.3. This could be caused by less heat generation with a degraded performance of the electrolyzers. For both models, with and without bubble formation, the cooling water rises before 4 MW and then experiences a dip before reaching its maximal setpoint, see Figure 4.3 and 4.4. As this is unexpected, the variation in the cooling water could be caused by a numerical error in the model and should be further investigated.

The bubble coverage for each of the electrolyzers is also presented in Figure 4.5. The coverage increases for all the electrolyzers with increasing current densities until it reaches its maximum. Additionally, greater efficiency yields greater bubble coverage. Further research should also be done for the unexpected change in the bubble coverage at approximately 1.2 MW.

For the simulated capacities at 5 MW, 6 MW, and 7 MW, the Weibull distributions are presented, see Figure 4.8, 4.7, and 4.9 respectively. The distribution curves have the same shape, but with different average power generations ranging from 0.985 MW to 1.379 MW. Due to these low average power generations, larger capacities or a different location for the wind turbines should be considered.

The flexible and fixed constraints for each of the capacities at 5 MW, 6 MW, and 7 MW are further analyzed for the simulated data. Considering maximal setpoints for each of the capacities, the HTO decrease with increased power inputs which results in less downtime with greater capacities.

Additionally, for a capacity at 5 MW, maximal setpoints increase the total production in 2019 with 2.8% compared with minimal setpoints, see Table 4.1. Meanwhile, flexible setpoints increase production in 2019 with 60.2%. Thus, optimizing with flexible setpoints is advantageous.

The results of the flexible setpoints at different capacities, 5 MW, 6 MW, and 7 MW, are also considered in Table 4.1. Compared to flexible setpoints at 5 MW, the total production in 2019 increased by 15.3% at 6 MW and 27.8% at 7 MW. However, considering the cost of investing in greater capacities, production and installation at 5 MW is most profitable with a cost of capital greater than 7.241%. Finally, for further work, it is recommended to develop a dynamic model for the plant in order to examine the plant behavior and implement control structures.

# Bibliography

- [1] Iain Staffell Stefan Pfenninger. Renewables.ninja. URL <https://www.renewables.ninja/about>. Accessed 26.10.2022.
- [2] Johannes Jäschke Lucas Cammann. *Comparing operational strategies for alkaline electrolysis systems considering a probabilistic wind power distribution*. PhD thesis, submitted to; Proceedings of the 33rd European Symposium on Computer Aided Process Engineering (ESCAPE33), 2023.
- [3] Inkscape’s Contributors and The Inkscape project. Inkscape, draw freely. URL <https://inkscape.org/about/>. Accessed 29.11.2022.
- [4] Md. Rizwan. Plantwide control of alkaline water electrolyzer plant for hydrogen production. Master’s thesis, Norwegian University of Sciences and Technology, Faculty of Natural Sciences, Department of Chemical Engineering, Trondheim, 2020.
- [5] James Galloway Zibigniew Klimont Wilfried Winiwarter Jan Willem Erisman, Mark A. Sutton. How a century of ammonia synthesis changed the world. *Nature Geoscience*, pages 636–639, 2008.
- [6] Sverre AAM. Energikrisa: Hva blir fremtidig gasspris i eu? URL <https://blogg.sintef.no/sintefenergy-nb/energikrisa-hva-blir-fremtidig-gasspris-i-eu/>. Accessed 12.12.2022.
- [7] Peter Ripson Hans van’t Noordende. A one-gigawatt green-hydrogen plant. URL <https://ispt.eu/media/Public-report-gigawatt-advanced-green-electrolyser-design.pdf>. Accessed 06.11.2022.
- [8] Thomas Turek Jörn Brauns. Alkaline water electrolysis powered by renewable energy: A review. *processes*, 8:1–23, 2020.
- [9] Øystein Ulleberg. Modeling of advanced alkaline electrolyzers: a system simulation approach. *International Journal of Hydrogen Energy*, (28):21–33, 2020.

- [10] Mitja Mori, Tilen Mržljak, Boštjan Drobnič, and Mihael Sekavčnik. Integral characteristics of hydrogen production in alkaline electrolyzers. *Strojniški vestnik-Journal of Mechanical Engineering*, 59(10):585–594, 2013.
- [11] Z.N. Vrontisi A.G. Tsikalakis. Vulnerability of energy to climate: Loss reduction by reactive power compensation. *Climate Vulnerability*, Chapter 3. Fuel Cell Electrochemistry:33–69, 2013.
- [12] Thomas Turek Jörn Brauns. Experimental evaluation of dynamic operating concepts for alkaline water electrolyzers powered by renewable energy. *Elsevier*, 8:1–13, 2021.
- [13] Carlos Ocampo-Martinez Sánchez-Peña Martín David, Fernando Bianchi.  $h_2$  purity control of high-pressure alkaline electrolyzers. *Instituto Tecnológico Buenos Aires (ITBA) and Consejo Nacional de Investigaciones Científicas y Técnicas (CONICET), Ciudad Autónoma de Buenos Aires, Argentina*, pages 1–2.
- [14] Dongke Zhang Kai Zeng. Recent progress in alkaline water electrolysis for hydrogen production and applications. *Progress in Energy and Combustion Science*, 36:307–326, 2010.
- [15] R.J. Balzer H. Vogt. The bubble coverage of gas-evolving electrodes in stagnant electrolytes. *Electrochimica Acta, Science direct*, pages 1–7, 2004, Berlin, Germany.
- [16] H. Vogt. The actual current density of gas-evolving electrodes - notes on the bubble coverage. *Electrochimica Acta, SciVerse ScienceDirect*, pages 1–5, 2012, Berlin, Germany.
- [17] H. Vogt J. Eigeldinger. The bubble coverage of gas-evolving electrodes in a flowing electrolyte. *Electrochimica Acta*, pages 1–8, 2000, Berlin, Germany.
- [18] Vesa Ruukanen Antti Kosonen Jero Ahola Olli Bergmann Georgios Sakas, Alejandro Ibáñez-Rioja. Dynamic energy and mass balance model for an industrial alkaline water electrolyzer plant process. URL <https://www.sciencedirect.com/science/article/pii/S0360319921045110>. Accessed 10.11.2022.
- [19] D.M. Himmelblau. Solubilities of inert gases in water. URL <https://pubs.acs.org/doi/pdf/10.1021/je60005a003>. Accessed 10.09.2022.
- [20] Dr.Mahmood Moshfeghian. Compressor calculations: Rigorous using equation of state vs short method. URL <http://www.jmcampbell.com/tip-of-the-month/2011/11/compressor-calculations-rigorous-using-equation-of-state-vs-shortcut-method/>. Accessed 27.11.2022.
- [21] Think Ahead ACCA. All the benefits of wind power. URL <https://www.enelgreenpower.com/learning-hub/renewable-energies/wind-energy/advantages-wind-energy>. Accessed 01.12.2022.
- [22] Academia. Physics of wind turbine. URL [https://www.academia.edu/8699900/Physics\\_of\\_Wind\\_Turbine](https://www.academia.edu/8699900/Physics_of_Wind_Turbine). Accessed 01.12.2022.



- [23] Cheng Xiaojun Peng Xiaoyun Jiang Yingni, Yuan Xiuling. Wind potential assessment using the weibull model at the inner mongolia of china. URL <https://journals.sagepub.com/doi/epdf/10.1260/014459806779367509>. Accessed 20.11.2022.
- [24] Tomas Freyman. The internal rate of return, . URL <https://www.accaglobal.com/gb/en/student/exam-support-resources/foundation-level-study-resources/ffm/ffm-technical-articles/the-internal-rate-of-return.html>. Accessed 10.12.2022.
- [25] John Jagerson. How to calculate net present value (npv). URL <https://www.investopedia.com/ask/answers/032615/what-formula-calculating-net-present-value-npv.asp>. Accessed 27.11.2022.
- [26] Viral B. Shah Alan Edelman Jeff Bezanson, Stefan Karpinski. The julia programming language. URL <https://julialang.org/>.
- [27] Lucas Cammann. Electrolyzer mwe, github, github repository, 2022. URL [https://github.com/lcammann/Student-projects?fbclid=IwAR3ML1D3HOY7VCjJ\\_BRu-V-N2e8XOQSzvumB9dGDNaTUQYNyCpJtdY6nZxs](https://github.com/lcammann/Student-projects?fbclid=IwAR3ML1D3HOY7VCjJ_BRu-V-N2e8XOQSzvumB9dGDNaTUQYNyCpJtdY6nZxs). Accessed 19.08.2022.
- [28] GitHub. jump.dev/ipopt.jl, 2022. URL <https://github.com/jump-dev/Ipopt.jl>. Accessed 19.08.2022.
- [29] Stig Blome Bettina Olie Bjerkholdt Ragnar Lurås, Martin Torstveit. Desperat jakt etter meir straum - her jublar dei for vindmøllepark. URL <https://www.nrk.no/vestfoldogtelemark/desperat-jakt-etter-meir-straum--her-jublar-dei-for-vindmollepark-1.16174371>. Accessed 25.11.2022.
- [30] Sanja Pekic. Yara and linde to build green hydrogen plant in norway. URL <https://www.offshore-energy.biz/yara-and-linde-to-build-green-hydrogen-plant-in-norway/>. Accessed 10.11.2022.
- [31] H Vogt. The actual current density of gas-evolving electrodes—notes on the bubble coverage. *Electrochimica acta*, 78:183–187, 2012.
- [32] Dan Blewett. Wind turbine cost: How much? are they worth it in 2022? URL <https://weatherguardwind.com/how-much-does-wind-turbine-cost-worth-it/>. Accessed 20.11.2022.
- [33] Harry Morgan. Opinion | why market dynamics will reduce the average price of green hydrogen to \$1.50/kg by 2030, 2022. URL <https://www.rechargenews.com/energy-transition/opinion-why-market-dynamics-will-reduce-the-average-price-of-green-hydrogen-to-2-1-1292801>. Accessed 19.11.2022.

- [34] Tomas Freyman. Global renewable energy sector reaches tipping point, .  
URL <https://www.grantthornton.global/en/insights/articles/tipping-point-to-grid-parity/>. Accessed 20.11.2022.

# Appendix A

## Appendix

### A.1 Performance Parameters

The performance parameters are set in order to illustrate the degradation of the three electrolyzers. Electrolyzer 1 is the most efficient while electrolyzer 3 is at the end of its lifespan. The parameters are set according to Rizwan[4], see Table A.1.

**Table A.1:** The performance parameters implemented for each of the electrolyzers according to Rizwan[4].

Performance Parameter	Electrolyzer 1	Electrolyzer 2	Electrolyzer 3	Units
$t_1$	$-145.29 \cdot 10^{-4}$	$-145.29 \cdot 10^{-3}$	$-145.29 \cdot 10^{-3}$	$\text{m}^2/\text{A}$
$t_2$	11.794	11.794	11.794	$\text{m}^2\text{C}/\text{A}$
$t_3$	395.68	395.68	395.68	$\text{m}^2\text{C}^2/\text{A}$
$r_1$	$2.18 \cdot 10^{-4}$	$2.62 \cdot 10^{-4}$	$2.84 \cdot 10^{-4}$	$\Omega\text{m}^2$
$r_2$	$-4.25 \cdot 10^{-7}$	$-4.25 \cdot 10^{-7}$	$-4.25 \cdot 10^{-7}$	$\Omega\text{m}^2/\text{C}$
$s$	$117.93 \cdot 10^{-3}$	$141.52 \cdot 10^{-3}$	$153.31 \cdot 10^{-3}$	V
$f_1$	120	144	156	$\text{mA}/\text{cm}^4$
$f_2$	0.98	0.97	0.96	–

### A.2 Julia Code

Only the main files and functions from Julia are included in this appendices[26].

#### A.2.1 Main

```
#Use relevant packages
using JuMP, Ipopt, Plots, PGFPlotsX, LaTeXStrings, Integrals, MTH229
```

```

#SSE1 = JuMP.Model(solver=Ipopt=Ipopt.IpoptSolver(max_iter=5000))

#Include necessary files and functions
include("Parameters.jl")
include("Model.jl")
include("Simulation.jl")
include("probability.jl")
include("eff.jl")
include("addExcelWind.jl")

#Define simulation settings

np = 40; #Points to consider in the simulation
Pnet = LinRange(30000,6.5e6,np); #Vector of power supply, in W
#np = 1;
#Pnet = 3e4;

# set the lye flowrate and the pressure constraints to
# lower/upper/optimal
cm = "optimal"; # constraint flowrate
cp = "optimal"; # constraint pressure
# set the model with/without bubble formation: "true"/"false"
bubbles = "true";
#Run simulationstring
sol, SSE1, ter, vals, startpoint, obj, tol = Simulation(np, par, Pnet,
cm, cp, bubbles)

## weighted #### -----

weighted = Array{Float64}(undef,np);
v = Array{Float64}(undef,np);

λ = 6.779;
k = 2.391;

Ablade = (2*10^6)/(0.5*par[:pair]*λ^3*log(10)^(3/k));

@syms Pwind

v = ((Pwind/(0.5*par[:pair]*Ablade))^(1/3));

functionofweight(Pwind) = (k/λ)*(((Pwind/(0.5*par[:pair]*Ablade))^(1/3))/λ)
^(k-1))*exp(-((Pwind/(0.5*par[:pair]*Ablade))^(1/3))/λ)^k);

for i=1:np
    weighted[i]= integrate(functionofweight(Pwind), (Pwind, 0, Pnet[i]));
end

#Plot results
# Absolute production rate
p01 = plot(Pnet, obj, title = "Absolute production rate",
label = L"Optimal point", shape = :circle, xlabel = L"P_{net} [W]",
ylabel = L"\dot{n}_{H2,out}\;[mols^{-1}]", framestyle
=:box, widen = false)
display(p01)

```

```

# Weighted production rate
p02 = plot(Pnet, weighted.*obj, title = "Weighted production rate",
label = L"Optimal\; point", shape = :circle, xlabel = L"P_{net} [W]",
ylabel = L"\bar{\dot{n}}_{H2,out}\;[mols^{-1}]",
framestyle =:box, widen = false)
display(p02)
# -----

mcw=26.6;
# behaviour of the optimization results
#1.
p1 = plot(Pnet/1e6, sol["P"]/par[:maxP], ylims=(0,1.1), title =
"Active constraint region, Electrolyzer 1",
titlefont=font(14), xguidefontsize = 16, yguidefontsize = 18,
legend = :outertopright, label = L"P", shape = :circle,
xlabel = L"Pnet\;[MW]", ylabel = L"g/g_{max}",
xtickfont=font(12), ytickfont=font(12),
legendfont = font(12), framestyle =:box, widen = false)
plot!(Pnet/1e6, sol["n_a_H2_o[1]"]./sol["n_sepa_O2_o[1]"]*100/2,
ylims=(0,1.1), label = L"HTO", shape = :circle)
plot!(Pnet/1e6, sol["m_cw[1]"]/mcw, label = L"\dot{m}_{cw}",
shape = :circle)
plot!(Pnet/1e6, sol["TEl[1]"]/(273+80), label = L"T^{E1}",
shape = :circle)
plot!(Pnet/1e6, sol["mel_lye_i[1]"]/(par[:maxlye]), label =
L"\dot{m}_{lye}", shape = :circle)
#plot!(size = (700,500))
display(p1)

#2.
p2 = plot(Pnet/1e6, sol["P"]/par[:maxP], ylims=(0,1.1), title =
"Active constraint region, Electrolyzer 2", titlefont=font(14),
xguidefontsize = 16, yguidefontsize = 18, legend = :outertopright,
label = L"P", shape = :circle, xlabel = L"Pnet\;[MW]",
ylabel = L"g/g_{max}", xtickfont=font(12), ytickfont=font(12),
legendfont = font(12), framestyle =:box, widen = false)
plot!(Pnet/1e6, sol["n_a_H2_o[2]"]./sol["n_sepa_O2_o[2]"]*100/2,
label = L"HTO", shape = :circle)
plot!(Pnet/1e6, sol["m_cw[2]"]/mcw, label = L"\dot{m}_{cw}",
shape = :circle)
plot!(Pnet/1e6, sol["TEl[2]"]/(273+80), label = L"T^{E1}",
shape = :circle)
plot!(Pnet/1e6, sol["mel_lye_i[2]"]/(par[:maxlye]), label =
L"\dot{m}_{lye}", shape = :circle)
display(p2)

#3.
p3 = plot(Pnet/1e6, sol["P"]/par[:maxP], ylims=(0,1.1), title =
"Active constraint region,
Electrolyzer 3", titlefont=font(14), xguidefontsize = 16,
yguidefontsize = 18, legend = :outertopright, label = L"P",
shape = :circle, xlabel = L"Pnet\;[MW]", ylabel = L"g/g_{max}",
xtickfont=font(12), ytickfont=font(12), legendfont = font(12),
framestyle =:box, widen = false)
plot!(Pnet/1e6, sol["n_a_H2_o[3]"]./sol["n_sepa_O2_o[3]"]*100/2,
label = L"HTO", shape = :circle)

```

```

plot!(Pnet/1e6, sol["m_cw[3]"]/mcw, label = L"\dot{m}_{cw}",
      shape = :circle)
plot!(Pnet/1e6, sol["TEl[3]"]/(273+80), label = L"T^{E1}",
      shape = :circle)
plot!(Pnet/1e6, sol["me1_lye_i[3]"]/(par[:maxlye]), label =
L"\dot{m}_{lye}", shape = :circle)
display(p3)

if bubbles == "true"
    p4 = plot(Pnet/1e6, sol[" $\theta$ [1]"], title="Bubble coverage,  $\theta$ ",
             titlefont=font(14), label = L" $\theta$ [1]", xlabel =
L"Pnet\[MW]", ylabel = L" $\theta$ ", framestyle =:box,
             legend = :outertopright,
             linewidth = 2, xguidefontsize = 16, yguidefontsize
             = 18, xtickfont=font(10),
             ytickfont=font(10), legendfont = font(13))
    plot!(Pnet/1e6, sol[" $\theta$ [2]"], label = L" $\theta$ [2]", linewidth = 2)
    plot!(Pnet/1e6, sol[" $\theta$ [3]"], label = L" $\theta$ [3]", linewidth = 2)
    display(p4)
    savefig(p4, "bubble.png");

    # saving active constraint regions
    savefig(p1, "E1Bt.png");
    savefig(p2, "E2Bt.png");
    savefig(p3, "E3Bt.png");

elseif bubbles == "false"
    # saving active constraint regions
    savefig(p1, "E1Bf.png");
    savefig(p2, "E2Bf.png");
    savefig(p3, "E3Bf.png");

end

```

## A.2.2 Model

```

function Build_Model(par,eff,startpoint,tol, iter, cm, cp, bubbles)
    SSE1 = Model(Ipopt.Optimizer)
    set_optimizer_attribute(SSE1, "max_iter", iter)
    set_optimizer_attribute(SSE1, "tol", tol)

    ##### Variables #####
    @variable(SSE1, Tbuff, start = startpoint[1,end]);
    @variable(SSE1, 10+273 <= TEl[n = 1:3] <= 80+273, start = startpoint[n+1,
end]);
    @variable(SSE1, I[n = 1:3], start = startpoint[n+4,end]); # current
    @variable(SSE1, U_rev, start = startpoint[8,end]); # -voltage
    @variable(SSE1, U, start = startpoint[9,end]);
    # MASS BALANCE - electrolyzers

```

```

@variable(SSE1, 0 <= n_H2_i[n = 1:3], start = startpoint[n+9,end])
@variable(SSE1, 0 <= n_O2_i[n = 1:3], start = startpoint[n+12,end]);
@variable(SSE1, 0 <= n_c_H2_o[n = 1:3], start = startpoint[n+15,end]);
@variable(SSE1, 0 <= n_a_H2_o[n = 1:3], start = startpoint[n+18,end]);
@variable(SSE1, 0 <= n_c_O2_o[n = 1:3], start = startpoint[n+21,end]);
@variable(SSE1, 0 <= n_a_O2_o[n = 1:3], start = startpoint[n+24,end]);
# SEPARATORS
@variable(SSE1, 0 <= n_sepa_H2_o[n = 1:3], start = startpoint[n+27,end]);
@variable(SSE1, 0 <= n_sepa_O2_o[n = 1:3], start = startpoint[n+30,end]);
@variable(SSE1, 0 <= n_sepc_H2_o[n = 1:3], start = startpoint[n+33,end]);
@variable(SSE1, 0 <= n_sepc_O2_o[n = 1:3], start = startpoint[n+36,end]);
# TEMPERATURES
@variable(SSE1, TE1_i[n = 1:3], start = startpoint[n+39,end]);
@variable(SSE1, Tcw_o[n = 1:3], start = startpoint[n+42,end]);
# MASS STREAMS
##### Configurations 1,2,3 #####
# Lower constraints
if cm == "lower"
@variable(SSE1, par[:minlye]*0.99 <= mel_lye_i[n = 1:3] <= par[:minlye]
*1.01, start = startpoint[n+45,end]);
@variable(SSE1, par[:minlye]*0.99 <= mel_lye_o[n = 1:3] <= par[:minlye]
*1.01, start = startpoint[n+48,end]);
@variable(SSE1, par[:minlye]*0.99 <= mbu_lye_i[n = 1:3] <= par[:minlye]
*1.01, start = startpoint[n+51,end]);
end
if cp == "lower"
@variable(SSE1, par[:minP]*0.99 <= P <= par[:minP]*1.01, start =
startpoint[55,end]);
end

# Upper constraints
if cm == "upper"
@variable(SSE1, par[:maxlye]*0.99 <= mel_lye_i[n = 1:3] <= par[:maxlye]*1.01,
start = startpoint[n+45,end]);
@variable(SSE1, par[:maxlye]*0.99 <= mel_lye_o[n = 1:3] <= par[:maxlye]*1.01,
start = startpoint[n+48,end]);
@variable(SSE1, par[:maxlye]*0.99 <= mbu_lye_i[n = 1:3] <= par[:maxlye]*1.01 ,
start = startpoint[n+51,end]);
end
if cp == "upper"
@variable(SSE1, par[:maxP] <= P <= par[:maxP], start = startpoint[55,end]);
end

# Optimal value
if cm == "optimal"
@variable(SSE1, par[:minlye] <= mel_lye_i[n = 1:3] <= par[:maxlye], start =
startpoint[n+45,end]);
@variable(SSE1, par[:minlye] <= mel_lye_o[n = 1:3] <= par[:maxlye], start =
startpoint[n+48,end]);
@variable(SSE1, par[:minlye] <= mbu_lye_i[n = 1:3] <= par[:maxlye] , start =
startpoint[n+51,end]);
end
if cp == "optimal"
@variable(SSE1, par[:minP] <= P <= par[:maxP], start = startpoint[55,end]);
end
#####
# 26.6

```

```

@variable(SSE1, 0.001 <= m_cw[n = 1:3] <= 26.6, start = startpoint[n+55,end]);
@variable(SSE1, 0 <= mmu_H2O <= 5, start = startpoint[59,end]); #Water makeup
#@variable(SSE1,  $\theta$ [n = 1:3], start = startpoint[n+59,end]);

##### Expressions #####
if bubbles == "true"
@variable(SSE1,  $\theta$ [n = 1:3], start = startpoint[n+59,end]);
@NLexpression(SSE1, nf[n = 1:3], eff[:f2,n]*((I[n]*(1- $\theta$ [n]))^2)/
(eff[:f1,n] + ((I[n]*(1- $\theta$ [n]))^2)));
@NLexpression(SSE1, n_r_H2[n = 1:3], nf[n]*((I[n]*(1- $\theta$ [n])*par[:ael])/
(2*par[:F]));
@NLexpression(SSE1, n_r_O2[n = 1:3], nf[n]*((I[n]*(1- $\theta$ [n])*par[:ael])/
(4*par[:F]));
elseif bubbles == "false"
@NLexpression(SSE1, nf[n = 1:3], eff[:f2,n]*((I[n]^2)/(eff[:f1,n] +
(I[n])^2)));
@NLexpression(SSE1, n_r_H2[n = 1:3], nf[n]*((I[n]*par[:ael])/
(2*par[:F]));
@NLexpression(SSE1, n_r_O2[n = 1:3], nf[n]*((I[n]*par[:ael])/
(4*par[:F]));
end
#@expression(SSE1, n_r_H2[n = 1:3], I[n]*(1- $\theta$ [n])*par[:ael]/(2*par[:F]));
#@expression(SSE1, n_r_O2[n = 1:3], I[n]*(1- $\theta$ [n])*par[:ael]/(4*par[:F]));
@expression(SSE1, S_H2, 1000/(0.018*7.1698*10^4)/(10^(3.14*0.312)));
@expression(SSE1, S_O2, S_H2*0.5);

@NLexpression(SSE1, n_diff_H2[n = 1:3], P*S_H2*par[:DH2]/(6.18*500e-6)
*par[:ael]);
@NLexpression(SSE1, n_diff_O2[n = 1:3], P*S_O2*par[:DH2]/(6.18*500e-6)
*par[:ael]);
@NLexpression(SSE1, n_buff_O2_i[n = 1:3], (0.5)*mbu_lye_i[n]*S_O2*P/
(par[:sepeff]*par[:rhol])); # Recycle to buffer tank eq. (1.19)
@NLexpression(SSE1, n_buff_H2_i[n = 1:3], (0.5)*mbu_lye_i[n]*S_H2*P/
(par[:sepeff]*par[:rhol]));

@NLexpression(SSE1, TEL_avg, (sum(mbu_lye_i[n]*TEL[n] for n in 1:3)
*par[:cpl])/(sum(mbu_lye_i[n] for n in 1:3)*par[:cpl])); # - H -
@NLexpression(SSE1, TEL_i_avg, sum(TEL_i[n]*mel_lye_i[n]*par[:cpl]
for n = 1:3)
/sum(mbu_lye_i[n]*par[:cpl] for n = 1:3));

@NLexpression(SSE1, Pcomp[n = 1:3], (n_sepc_H2_o[n] +
n_sepa_O2_o[n])/par[:effcomp]*(1.4/0.4)*8.314*TEL[n]*((25/P)^
(0.4/1.4)-1));
@expression(SSE1, logT[n = 1:3], (Tbuff + TEL_i[n])/2 - (Tcw_o[n] +
par[:Tcw])
/2)
@NLexpression(SSE1, HTO[n = 1:3], n_a_H2_o[n]/n_sepa_O2_o[n]);
@NLexpression(SSE1, etasys[n = 1:3], n_c_H2_o[n]*par[:LHV]*1e6/
(par[:U]*I[n]*par[:ael]+Pcomp[n]));
@NLexpression(SSE1, v[n = 1:3], mel_lye_i[n]/(par[:rhol]*3.63*
0.1));

@NLexpression(SSE1, tot, sum(n_sepc_H2_o[n] for n in 1:3));
@NLexpression(SSE1, mbu_lye_i_tot, sum(mbu_lye_i[n] for n in 1:3));
@NLexpression(SSE1, mel_lye_o_tot, sum(mel_lye_o[n] for n in 1:3));

```



```

@NLexpression(SSE1, mel_lye_i_tot, sum(mel_lye_i[n] for n in 1:3));
@NLexpression(SSE1, n_buff_H2_i_tot, sum(n_buff_H2_i[n] for n in
1:3));
@NLexpression(SSE1, n_H2_i_tot, sum(n_H2_i[n] for n in 1:3));
@NLexpression(SSE1, n_buff_O2_i_tot, sum(n_buff_O2_i[n] for n in
1:3));
@NLexpression(SSE1, n_O2_i_tot, sum(n_O2_i[n] for n in 1:3));

##### Model (written as constraints) #####
# Starting with Ullebergs model
@NLconstraint(SSE1, Urev, U_rev - (1.5184 - 1.5421e-3*TEL_avg +
9.523e-5*TEL_avg*log(TEL_avg) + 9.84e-8*TEL_avg^2) == 0);
@NLconstraint(SSE1, Eb_el, mel_lye_i_tot*par[:cpl]*(TEL_i_avg -
TEL_avg) + (U -par[:Utn])*sum(I[n] for n in 1:3)*(par[:ael]) - par[:as]
*(par[:hc]*(TEL_avg-293) + par[:sb]*par[:emis]*(TEL_avg^4 - 293^4)
== 0);
# Different efficiencies for the electrolyzers
@NLconstraint(SSE1, Uex[n = 1:3], (U - U_rev) - ((eff[(:r1,n)] +
eff[(:r2,n)]*(TEL[n]-273))*I[n] + eff[(:s,n)]*log10((eff[(:t1,n)]
+ eff[(:t2,n)]/(TEL[n]-273)
+eff[(:t3,n)]/(TEL[n]-273)^2)*I[n]+1)) == 0);

#Additional model equations
#Electrolyzer
@NLconstraint(SSE1, [n = 1:3], n_H2_i[n] + n_r_H2[n] - n_diff_H2[n] -
n_c_H2_o[n] == 0);
@NLconstraint(SSE1, [n = 1:3], n_O2_i[n] + n_diff_O2[n] - n_c_O2_o[n]
== 0);
@NLconstraint(SSE1, [n = 1:3], n_H2_i[n] + n_diff_H2[n] - n_a_H2_o[n]
== 0);
@NLconstraint(SSE1, [n = 1:3], n_O2_i[n] + n_r_O2[n] - n_diff_O2[n] -
n_a_O2_o[n] == 0);
@NLconstraint(SSE1, [n = 1:3], par[:MH2]*(2*n_H2_i[n] - n_c_H2_o[n] -
n_a_H2_o[n]) + par[:MO2]*(2*n_O2_i[n] - n_c_O2_o[n] - n_a_O2_o[n])
+ mel_lye_i[n] - mel_lye_o[n] == 0);
#Separators
@NLconstraint(SSE1, [n = 1:3], n_a_H2_o[n] - n_sepa_H2_o[n] == 0);
@NLconstraint(SSE1, [n = 1:3], n_a_O2_o[n] - n_sepa_O2_o[n] -
n_buff_O2_i[n] == 0);
@NLconstraint(SSE1, [n = 1:3], n_c_H2_o[n] - n_sepc_H2_o[n] -
n_buff_H2_i[n] == 0);
@NLconstraint(SSE1, [n = 1:3], n_c_O2_o[n] - n_sepc_O2_o[n] == 0);
@NLconstraint(SSE1, [n = 1:3], par[:MH2]*(n_a_H2_o[n] - n_sepa_H2_o[n]) +
par[:MO2]*
(n_a_O2_o[n] - n_sepa_O2_o[n] - n_buff_O2_i[n]) + (0.5)*mel_lye_o[n] -
(0.5)*mbu_lye_i[n] == 0);
@NLconstraint(SSE1, [n = 1:3], par[:MH2]*(n_c_H2_o[n] - n_sepc_H2_o[n] -
n_buff_H2_i[n])
+ par[:MO2]*(n_c_O2_o[n] - n_sepc_O2_o[n]) + (0.5)*mel_lye_o[n] - (0.5)*
mbu_lye_i[n] == 0);

#Buffer tank
@NLconstraint(SSE1, n_buff_H2_i_tot - 2*n_H2_i_tot == 0);
@NLconstraint(SSE1, n_buff_O2_i_tot - 2*n_O2_i_tot == 0);
@NLconstraint(SSE1, mbu_lye_i_tot + mmu_H2O - mel_lye_i_tot + par[:MH2]*(
n_buff_H2_i_tot - 2*n_H2_i_tot) + par[:MO2]*(n_buff_O2_i_tot - 2*n_O2_i_tot)

```

```

== 0);
@NLconstraint(SSE1, mbu_lye_i_tot*par[:cpl]*(TEl_avg - par[:T0]) + mmu_H2O*
par[:cph20]*(par[:Tcw] - par[:T0]) - mel_lye_i_tot*par[:cpl]*(Tbuff -
par[:T0]) == 0);
#HEX
@NLconstraint(SSE1, [n = 1:3], mel_lye_i[n]*par[:cpl]*(Tbuff - TEl_i[n]) -
par[:UHX]*logT[n] == 0);
@NLconstraint(SSE1, [n = 1:3], m_cw[n]*par[:cph20]*(par[:Tcw] - Tcw_o[n]) +
par[:UHX]*logT[n] == 0);

#Additional model constraints
@constraint(SSE1, [n = 1:3], -20 <= TEl[n] - TEl_i[n] <= 20);
@NLconstraint(SSE1, [n = 1:3], HTO[n]*100 <= 2);
@NLconstraint(SSE1, 0 <= U*sum(I[n] for n in 1:3)*(par[:ael]) +
sum(Pcomp[n] for n in 1:3) <= par[:Pnet]);
if bubbles == "true"
@NLconstraint(SSE1, [n = 1:3],  $\theta[n] - (I[n]/(3.08*par[:jlim]))^{(0.3)}/$ 
 $(1+(8*v[n])^2)^2 == 0$ );
end

#Objective
@NLobjective(SSE1, Max, tot);
return SSE1
end

```

## A.3 Simulation

```

function Simulation(np,par,Pnet, cm, cp, bubbles)

# fist starts values
s = [350, # 1 # Tbuff
50+273, 50+273, 50+273, # 2-4 # TEl
500, 500, 500, # 5-7 # I
1.4, # 8 # Urev
0, # 9 # U
1, 1, 1, # 10-12 # n_H2_i
1, 1, 1, # 13-15 # n_O2_i
1, 1, 1, # 16-18 # n_c_H2_o
0.01, 0.01, 0.01, # 19-21 # n_a_H2_o
0.01, 0.01, 0.01, # 22-24 # n_c_O2_o
1, 1, 1, # 25-27 # n_a_O2_o
0.01, 0.01, 0.01, # 28-30 # n_sepa_H2_o
1, 1, 1, # 31-33 # n_sepa_O2_o
0.01, 0.01, 0.01, # 34-36 # n_sepc_H2_o
1, 1, 1, # 37-39 # n_sepc_O2_o
340, 340, 340, # 40-42 # TEl_i
305, 305, 305, # 43-45 # Tcw_o
10, 10, 10, # 46-48 # mel_lye_i
9.9, 9.9, 9.9, # 49-51 # mel_lye_o
9.9, 9.9, 9.9, # 52-54 # mby_lye_i

```

```

4, # 55 # P
5, 5, 5, # 56-58 # m_cw
0.1]; # 59 # mmu_H2O
#1, 1, 1]; # 60-62 # theta

if bubbles == "true"
    push!(s,1);
    push!(s,1);
    push!(s,1);
end

# tolerance of Ipopt
tol = 1e-8;
iter = 10000;

#Prepare the simulation
SSE1 = Build_Model(par, eff, s, tol, iter, cm,cp, bubbles)
nvars = length(all_variables(SSE1))

#Pre-allocate arrays and vectors
vars = Vector{VariableRef}(undef,nvars);
vals = Array{Float64}(undef,nvars,np);
ter = Vector{Any}(undef,np);
obj = Array{Float64}(undef,np);

startpoint = Matrix{Float64}(undef, nvars, np);
startpoint[:,1] = s;

for i in 1:np
    global vars, sol
    par[:Pnet] = Pnet[i]
    ## Setting up JuMP model
    SSE1 = Build_Model(par, eff, startpoint[:, i], tol, iter,cm,cp,
    bubbles)
    optimize!(SSE1)

    #Save values of variables
    ter[i] = termination_status(SSE1)

    if ter[i] == ALMOST_LOCALLY_SOLVED::TerminationStatusCode
        tol = 1e-4;
        iter = 10000;
        SSE1 = Build_Model(par, eff, startpoint[:, i], tol, iter,
        cm,cp,bubbles)
        optimize!(SSE1)
    elseif ter[i] == ITERATION_LIMIT::TerminationStatusCode
        tol = 1e-8;
        iter = 100000;
        SSE1 = Build_Model(par, eff, startpoint[:, i], tol, iter,
        cm,cp,bubbles)
        optimize!(SSE1)
    end

    vars = name.(all_variables(SSE1))
    vals[:, i] = value.(all_variables(SSE1))
end

```

```

    j = i+1;
    if j <= np
        startpoint[:,j] = vals[:,i];
    end
    if i == 1
        sol = Dict(vars[1] => vals[1,:])
    end
    for j in 2:nvars
        push!(sol, vars[j] => vals[j,:])
    end

    obj[i] = objective_value(SSE1);

end
return sol, SSE1, ter, vals, startpoint, obj, tol
end

```

### A.3.1 Parameters

```

par = Dict{Symbol,Float64}(:U => 1.6,
:Tin => 273+60,
:qly => 2,
:qcw => 6,
:Pnet => 1e6,
:Urev => 1.2,
:Utn => 1.482,
:jlum => 7500, # current => decreasing current densities creates more bubble coverage
:k => 1e-4,
:rho1 => 1258.2,
:cpl => 3101,
:cph20 => 4186,
:eps => 0.8,
:sig => 5.67e-8,
:hc => 5.5,
:nc => 230,
:ael => 2.6*230, #Caution! Needs to be updated when nc changes
:V => 5.98, #0.01m * ael
:as => 131.56,
:utn => 1.482,
:F => 96485,
:cH2s => 0.056,
:cO2s => 6.4e-4,
:DH2 => 5.38e-9,
:DO2 => 2e-9, #Guessed! Use correlation for exact numerical value
:Tin => 273+80,
:sb => 5.67e-8,
:emis => 0.8,
:dsep => 500e-6,
:djsb => 187e-6,
:vO2 => 0.5,
:vH2 => 1,

```

```

:p => 1,
:sepeff => 0.99,
:effcomp => 0.8,
:Tcw => 273+20,
:UHX => 5000,
:MH2 => 0.002,
:MO2 => 0.032,
:T0 => 273,
:headP => 9,
:minP => 2,
:maxP => 25,
:minlye => 1,
:maxlye => 30, #kg/s, roughly 10 times recycled per hour equals 40
:rhoair => 1.225,
:LHV => 0.24, #MJ/0.002 kg H2 (per 1 mole)
:A => 2.6,
:λ => 6.779,
:kp => 3.391,
:ρair => 1.225);

```

### A.3.2 Performance parameters

```

eff = Dict{Tuple{Symbol, Int64},Float64}({
# efficiencies (life cycle) of the electrolyzers:
(:r1,1) => 2.18e-4,
(:r2,1) => -4.25e-7,
(:s,1) => 117.93e-3,
(:t1,1) => -145.29e-3,
(:t2,1) => 11.794,
(:t3,1) => 395.68,
(:f1,1) => 120.0,
(:f2,1) => 0.98,
# -----
(:r1,2) => 2.62e-4,
(:r2,2) => -4.25e-7,
(:s,2) => 141.52e-3,
(:t1,2) => -145.29e-3,
(:t2,2) => 11.794,
(:t3,2) => 395.68,
(:f1,2) => 144.0,
(:f2,2) => 0.97,
# -----
(:r1,3) => 2.84e-4,
(:r2,3) => -4.25e-7,
(:s,3) => 153.31e-3,
(:t1,3) => -145.29e-3,
(:t2,3) => 11.794,
(:t3,3) => 395.68,
(:f1,3) => 156.0,
(:f2,3) => 0.96);
# -----

```

### A.3.3 The net present value

```

function NPV(MW, P, r, N)
  # For one project:
  # MW: installed wind turbines with capacity of 5, 6 or 7[MW]
  # P: production of hydrogen [kg/year]
  # r: discount rate
  # N: years

  F = 3.7*P;          # dollar/kg * kg/year
  C0 = 1300000*MW;   # installation cost [dollar/MW] * MW

  CF = 0;
  for n in 1:N
    CF += F/((1+r)^n);
  end

  #print(CF)

  npv = -C0 + CF;

  return npv
end

#NPV(5,obj_year(obj_net50), 0, 25)

```

### A.3.4 Wind data

```

function addExcelWind(Excel)
  # Data from Herøya 2019 - 6000 capacity + raw data
  xr = XLSX.readxlsx(Excel)

  data = XLSX.readdata(Excel, Excel, "A5:A8764")

  nr = length(data);

  wind_speed = Array{Float64}(undef,nr); # speed
  str_speed = Array{String}(undef,nr);
  wind_power = Array{Float64}(undef,nr); # power
  str_power = Array{String}(undef,nr);

  for i in 1:nr

    if length(data[i]) == 49
      str_speed[i] = data[i][:(nextind.(data[i], 0,
        (44,49))...)];
      wind_speed[i] = parse(Float64,str_speed[i]);
      str_power[i] = data[i][:(nextind.(data[i], 0,

```

```

        (35,42)...)];
        wind_power[i] = parse(Float64, str_power[i]);
    elseif length(data[i]) == 48
        str_speed[i] = data[i][:(nextind.(data[i], 0,
            (44,48))...)];
        wind_speed[i] = parse(Float64, str_speed[i]);
        str_power[i] = data[i][:(nextind.(data[i], 0,
            (35,42))...)];
        wind_power[i] = parse(Float64, str_power[i]);
    elseif length(data[i]) == 47
        str_speed[i] = data[i][:(nextind.(data[i], 0,
            (43,47))...)];
        wind_speed[i] = parse(Float64, str_speed[i]);
        str_power[i] = data[i][:(nextind.(data[i], 0,
            (35,41))...)];
        wind_power[i] = parse(Float64, str_power[i]);
    elseif length(data[i]) == 46
        str_speed[i] = data[i][:(nextind.(data[i], 0,
            (42,46))...)];
        wind_speed[i] = parse(Float64, str_speed[i]);
        str_power[i] = data[i][:(nextind.(data[i], 0,
            (35,40))...)];
        wind_power[i] = parse(Float64, str_power[i]);
    elseif length(data[i]) == 45
        str_speed[i] = data[i][:(nextind.(data[i], 0,
            (41,45))...)];
        wind_speed[i] = parse(Float64, str_speed[i]);
        str_power[i] = data[i][:(nextind.(data[i], 0,
            (35,39))...)];
        wind_power[i] = parse(Float64, str_power[i]);
    else
        print(i)
        throw(error())
    end
end

wind_power = 1000*wind_power; # kW --> W

dailymeanspeed = Array{Float64}(undef, 365); # dailymeanspeed
dailymeanspeed[1] = sum(wind_speed[1:23])/23;

dailymeanspower = Array{Float64}(undef, 365); # dailymeanspower
dailymeanspower[1] = sum(wind_power[1:23])/23;

dstart = [24];
dend = [47];
for i in 2:365
    #global dstart, dend
    dailymeanspeed[i] = sum(wind_speed[dstart[1]:dend[1]])/24;
    dailymeanspower[i] = sum(wind_power[dstart[1]:dend[1]])/24;
    dstart[1] += 24;
    dend[1] += 24;
end
end

```

```

weeklymean_speed = Array{Float64}(undef, 52); # weekly mean
weeklymean_power = Array{Float64}(undef, 52); # weekly mean

wstart = [1];
wend = [7];

for i in 1:52
    #global wstart, wend
    weeklymean_speed[i] = (sum(wind_speed[wstart[1]:wend[1]])
/7); # m/s
    weeklymean_power[i] = (sum(wind_power[wstart[1]:wend[1]])
/7); # W
    wstart[1] += 7;
    wend[1] += 7;
end
#           1           2           3           4
return wind_power, wind_speed, weeklymean_power,
weeklymean_speed
end

```

### A.3.5 Absolute and Weighted production rate

```

function constrainttest(wind_speed, datapointspower, datapointsspeed,
cm, cp, bubbles)

# weekly production
Data = sort(datapointspower);
Data_speed = sort(datapointsspeed);
N = length(Data);

# Simulation
#np = 1;
ope = [0.0];
operate = Array{Float64}(undef, N);
obj_net = Array{Float64}(undef, N); # product, n
weighted = Array{Float64}(undef, N); # weighted
belowvelocity = Array{Float64}(undef, N);

#Run simulation
sol, SSE1, ter, vals, startpoint, obj, tol =
Simulation(N, par, Data, cp, cm, bubbles);

for i in 1:N

    if ter[i] == OPTIMAL::TerminationStatusCode || ter[i] ==
ALMOST_OPTIMAL::TerminationStatusCode ||
ter[i] == LOCALLY_SOLVED::TerminationStatusCode ||
ter[i] == ALMOST_LOCALLY_SOLVED::TerminationStatusCode
ope[1] = 1;
obj_net[i] = obj[i];

```



```
        belowvelocity[i] = 0;
    else
        ope[1] = 0;
        obj_net[i] = 0;
        belowvelocity[i] = Data_speed[i];
    end

    weighted[i] = weibull(Data, Data_speed)[2][i]*obj_net[i];

    operate[i] = ope[1];
end

# numerical integration of the absolute and weighted
# production rate; using the trapezodial rule
Trapzobj = trapz(Data, obj_net);
Trapzweigh = trapz(Data, weighted);

# minimum velocity
maxbelow = maximum(belowvelocity);
l = length(wind_speed);

# check velocity below minimum through the year
below = [0.0];
for i in 1:l

    if wind_speed[i] < maxbelow
        below[1] += 1;
    end
end
#      1      2      3      4
return obj_net, weighted, Trapzobj, Trapzweigh,
# 5      6
below, Data
end
```